Tréhu, A.M., Bohrmann, G., Torres, M.E., and Colwell, F.S. (Eds.)
Proceedings of the Ocean Drilling Program, Scientific Results Volume 204

1. Leg 204 Synthesis: Gas Hydrate Distribution and Dynamics in the Central Cascadia Accretionary Complex[1]

A.M. Tréhu,[2] M.E. Torres,[2] G. Bohrmann,[3] and F.S. Colwell[4]

ABSTRACT

Ocean Drilling Program (ODP) Leg 204 to Hydrate Ridge, located on the continental slope offshore Oregon (USA), was the first drilling expedition dedicated to understanding gas hydrate processes in accretionary complexes and provided a testbed for a number of different techniques for estimating the gas hydrate content of sediments. It was also the first time that (1) digital infrared scans of core temperature were systematically recorded for all cores from within or near the gas hydrate stability zone, facilitating identification of gas hydrate samples for further study, (2) hydrate-bearing cores were recovered and logged at in situ pressure, and (3) ODP allowed acquisition of logging-while-drilling data prior to coring at a given site, providing an initial comprehensive estimate of gas hydrate distribution that was used to design the subsequent coring program.

Gas hydrate estimates based on a variety of geophysical and geochemical techniques indicate a heterogeneous distribution of gas hydrate, which results in part because of two distinct regimes for delivery of gas to the gas hydrate stability zone. In the "reaction regime," which is pervasive throughout the study region, the average gas hydrate content of the sediments is relatively low (2%–8% of the pore space), no gas hydrate is present in the upper ~30 meters below seafloor (mbsf) because the methane content of the pore water is below saturation, and the fine-scale distribution of gas hydrate depends strongly on lithology. Superimposed on the reaction regime is a "transport-dominated re-

[1]Tréhu, A.M., Torres, M.E., Bohrmann, G., and Colwell, F.S., 2006. Leg 204 synthesis: gas hydrate distribution and dynamics in the central Cascadia accretionary complex. *In* Tréhu, A.M., Bohrmann, G., Torres, M.E., and Colwell, F.S. (Eds.), *Proc. ODP, Sci. Results,* 204: College Station, TX (Ocean Drilling Program), 1–40. doi:10.2973/odp.proc.sr.204.101.2006
[2]College of Oceanic and Atmospheric Sciences, Oregon State University, Corvallis OR 97331, USA. Correspondence author: **trehu@coas.oregonstate.edu**
[3]Research Center Ocean Margins, University of Bremen, D-28334 Bremen, Germany.
[4]Idaho National Laboratory, Idaho Falls ID 83415, USA. Present address: College of Oceanic and Atmospheric Sciences, Oregon State University, Corvallis OR 97331, USA.

Initial receipt: 22 March 2006
Acceptance: 4 September 2006
Web publication: 1 November 2006
Ms 204SR-101

gime" in which gas is focused into a stratigraphically controlled conduit and is transported as free gas to the structural summit. At the summit, high gas pressure drives free gas into and through the gas hydrate stability zone, resulting in a shallow deposit in which gas hydrate comprises ~25% of the total sediment volume to a depth of ~25 mbsf. Geochemical data indicate that most of the gas that forms the summit deposit has migrated from greater depth and has either a thermogenic or altered biogenic character, and modeling suggests that abundant free gas is needed to form gas hydrate in these conditions. Although this deposit contains only ~2% of the estimated total volume of methane trapped in gas hydrate within the study region, it may be particularly susceptible to destabilization in response to oceanographic change.

INTRODUCTION

Ocean Drilling Program (ODP) Leg 204, which focused on a topographic high in the Cascadia accretionary complex ~80 km west of Newport, Oregon (USA), and 15 km east of the current deformation front (Fig. **F1**), was the first ODP expedition dedicated to understanding gas hydrate in an accretionary complex. Leg 204 builds on the results of Deep Sea Drilling Project (DSDP) Leg 18 (Sites 174–176) (Kulm and von Huene, 1973) and ODP Leg 146 (Sites 888–892) (Westbrook, Carson, Musgrave, et al., 1994), which studied the process of sediment subduction and accretion on the Cascadia margin, and Leg 164, drilled on the Blake Ridge (Paull, Matsumoto, Wallace, et al., 1996), which was the first ODP leg dedicated to understanding gas hydrate processes. Leg 204 is complemented by Integrated Ocean Drilling Program (IODP) Expedition 311, which targeted a segment of the northern Cascadia margin that is characterized by coarse-grained trench sediments (Expedition 311 Scientists, 2005), in contrast to the finer-grained slope sediments that dominate the lithologies sampled during Leg 204 (Tréhu, Bohrmann, Rack, Torres, et al., 2003; **Su et al.,** this volume, **Gràcia et al.,** this volume).

Nine sites were occupied during Leg 204 (Table **T1;** Fig. **F2A**). The sites were located in water depths of 780–1210 meters below sea level (mbsl) near the southern part of Hydrate Ridge (SHR). All sites were located within a 4 km × 11 km region that was imaged to a subseafloor depth of ~1 km by three-dimensional (3-D) seismic data. The 3-D seismic data provide tectonic and stratigraphic links among the sites (Fig. **F2B–F2F**) and enable reconstruction of the geologic history (**Chevallier et al.,** this volume; Bangs et al., 2005). Logging-while-drilling (LWD) data acquired at the beginning of the leg provided initial estimates of the hydrate distribution as inferred from electrical resistivity anomalies. These estimates were used to plan the subsequent coring program.

Immediately after recovery, all cores from within the gas hydrate stability zone (GHSZ) were scanned with a track-mounted infrared camera to detect "cold spots" indicative of recent or ongoing dissociation of gas hydrate. The sections of core showing the strongest cold spots were sampled for shipboard experiments to calibrate geophysical proxies for gas hydrate presence or to preserve the gas hydrate for shore-based structural analyses. Gas hydrate presence was also determined based on a variety of geochemical and geophysical measurements (see **"Intercalibration of Different Gas Hydrate Proxies,"** p. 10). All shipboard data, with limited interpretation, were presented in the Leg 204 *Initial Reports* volume (Tréhu, Bohrmann, Rack, Torres, et al., 2003).

F1. DSDP Leg 18, ODP Legs 146 and 204, and IODP Expedition 311 sites, p. 26.

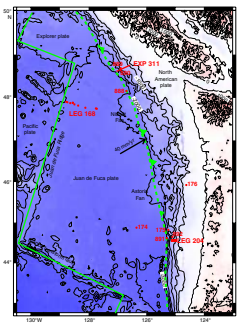

T1. Leg 204 site summaries, p. 37.

F2. Leg 204 sites, p. 27.

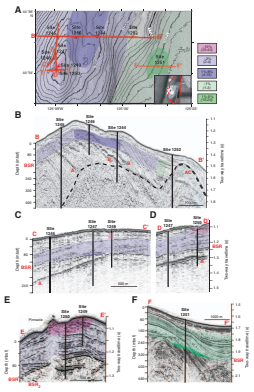

Gas hydrate presence was confirmed at all sites except for Site 1252, where the main seismic indicator for gas hydrate is also locally absent (Fig. F2B). The amount of gas hydrate present, when averaged over the entire thermodynamically defined GHSZ, is generally estimated to be ~2% of the sediment pore space (Milkov et al., 2003; Tréhu et al., 2004b). It increases to ~10% near methane vents at the southern summit of the ridge, where massive gas hydrate forms in the upper 20–30 meters below seafloor (mbsf) and occupies 20%–30% of the total volume. Gas hydrate is also locally abundant at some sites in clusters of discrete lenses that range from submillimeter to decimeter thickness and increase the average gas hydrate content of the sediment to up to 8% of the pore space (Fig. F2A) (Tréhu et al., 2004b). These estimates are significantly lower than some previous estimates for Cascadia (e.g., Hyndman et al., 2001). Differences between the earlier estimates and the estimates from Leg 204 can be attributed to uncertainties in the appropriate baselines used to interpret indirect proxies for gas hydrate content (Torres et al., 2004a; Riedel et al., 2005; see also "Intercalibration of Different Gas Hydrate Proxies," p. 10).

Two distinct modes of gas hydrate formation are recognized. Rich gas hydrate deposits form where abundant methane is transported from greater depth within the accretionary prism along discrete conduits (Torres et al., 2004b, 2005; Milkov and Xu, 2005; Liu and Flemings, 2006). At SHR, this conduit results primarily from an anomalously coarse-grained stratigraphic horizon (Tréhu et al., 2004a), labeled A in Figure F2. This mechanism focuses methane from a large region in the subsurface to a few seafloor vents. In the other mode, regionally pervasive gas hydrate forms from gas produced locally through microbial activity, exsolved from pore waters in response to tectonic uplift, and transported advectively through diffuse fluid flow. Superimposed on these two distinct modes of gas delivery to the GHSZ is the effect of lithology (Weinberger et al., 2005; Gràcia et al., this volume; Su et al., this volume), which affects gas hydrate nucleation and small-scale fluid transport (Clennell et al., 1999). Prediction of gas hydrate deposits thus requires an integrated geological, geochemical, and geophysical approach, similar to that used for prediction of conventional hydrocarbon resources.

The objective of this chapter is to summarize the primary results from publications based on data from Leg 204. We first discuss the geologic history of SHR, followed by a discussion of the factors that control the heterogeneous gas hydrate distribution. We then compare estimates of the gas hydrate distribution and amount derived from different geophysical and geochemical proxies with different precision and resolution and summarize other related studies of the physical properties and parameters of the host sediments. Finally, we consider the distribution and type of microbial communities present in the subsurface strata of SHR and compare those communities derived from sediments that contain gas hydrates to those derived from nearby sediments that lack gas hydrates.

GEOLOGIC HISTORY OF SOUTHERN HYDRATE RIDGE

The Juan de Fuca plate is currently being subducted obliquely beneath North America at the Cascadia subduction zone. Much of the 3-

to 4-km-thick sediment cover of the subducting plate is accreted to North America in the process, either by offscraping at the deformation front or by underplating beneath the accretionary complex some tens of kilometers east of the deformation front (MacKay et al., 1992; MacKay, 1995; **Johnson et al.,** this volume), resulting in a broad fold and thrust belt on the continental slope. Hydrate Ridge, a north-south-trending peanut-shaped structure, is one of these ridges. Since discovery of cold seeps and associated vent fauna on Hydrate Ridge two decades ago (Kulm et al., 1986), it has been the focus of many studies. A nearly ubiquitous bottom-simulating reflector (BSR) suggests that gas hydrate is widespread in the sediments of Hydrate Ridge (Tréhu et al., 1999). Seafloor manifestations of gas hydrate and associated authigenic carbonate, however, are more limited (e.g., Johnson et al., 2003).

The northern summit of Hydrate Ridge (NHR) is affected by widespread venting, as indicated by an extensive carbonate carapace (Bohrmann et al., 1998; Greinert et al., 2001; Johnson et al., 2003; Teichert et al., 2005a) and numerous sites where bubbles emerge from the seafloor (Heeschen et al., 2003). ODP Site 892, drilled during Leg 146, was located on the northern summit of Hydrate Ridge where an upward deflection of the BSR is cut by a fault (Shipboard Scientific Party, 1994). At this site, massive gas hydrates were recovered from 2 to 19 mbsf (Kastner et al., 1995). No hydrate was recovered from near the BSR, but pore water geochemical and temperature anomalies suggested the presence of disseminated hydrate in the pore space to 68 mbsf (Kastner et al., 1995; Hovland et al., 1995). Vertical seismic profiles (VSPs) and seismic refraction data indicate the presence of an extensive free gas zone beneath the gas hydrate stability zone (MacKay et al., 1994; Tréhu and Flueh, 2001). Methane at Site 892 is primarily of biogenic origin (Kvenvolden, 1995), but higher-order hydrocarbons of thermogenic origin are also present (Hovland et al., 1995). In contrast, seafloor manifestations of venting at SHR are limited to a single, 50-m-high carbonate pinnacle 250 m southwest of the summit and to a massive hydrate deposit and a single, persistent bubble plume at the summit (Suess et al., 1999, 2001; Torres et al., 2002; Heeschen et al., 2003; Tréhu et al., 1999, 2004b; Johnson et al., 2003).

The geologic history of Hydrate Ridge, which provides constraints on the origin of methane for forming gas hydrates and on the temporal evolution of these deposits, can be reconstructed from a series of seismic imaging experiments conducted as site surveys for Legs 146 and 204. The Leg 146 site survey, which included a series of seismic profiles spaced 1–3 km apart across the subduction zone deformation front and accretionary complex between 44.5°N and 45.5°N, indicates that Hydrate Ridge is located where the dominant vergence of thrusting at the deformation front changes from seaward to landward (MacKay et al., 1992; MacKay, 1995; **Johnson et al.,** this volume). This transition corresponds to a transition from accretion of all sediment on the incoming plate off northern Oregon and Washington (Fisher et al., 1999) to subduction of the lower half of the incoming sediment column.

Figure **F3** shows the deep structure beneath SHR. The deformation front is characterized by a distinct landward-dipping thrust fault that can be followed intermittently to a depth of ~7 km beneath the summit of Hydrate Ridge. The amount of underthrusting shown in Figure **F3B** corresponds to ~0.3 m.y. of subduction at the current oblique subduction rate of ~4 cm/yr, which is consistent with the estimate of 0.3 Ma for reactivation of uplift of SHR derived by **Chevallier et al.** (this volume) based on 3-D seismic and biostratigraphic (**Watanabe,** this volume) data from Leg 204. The cross-sectional area of the accretionary complex sedi-

F3. SHR seismic profile, section, and slice, p. 28.

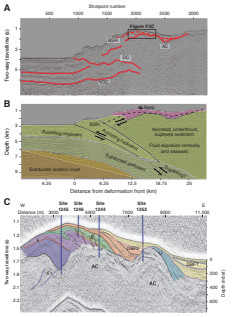

ments overlying the décollement represents approximately twice this amount of time, assuming constant incoming sediment thickness and subduction rate; this consistent with the estimate by **Chevallier et al.** (this volume) for the initiation of uplift of SHR at ~1 Ma.

Perhaps surprisingly, the thickness of the underthrust sediment package does not appear to decrease significantly arcward of the deformation front as would be expected because of compaction and sediment dewatering. In fact, it appears to thicken somewhat, suggesting either that the thickness of sediment on the subducting plate has decreased recently or that underthrust sediments are being tectonically thickened. Uplift of the accreted sediments by duplexing and underplating, and additional uplift of pore fluid through mechanical dewatering, contribute to gas hydrate formation because the solubility of methane near the base of the GHSZ in a water depth of 800 mbsl (i.e., at the summit of SHR) is ~50% of the solubility in a water depth of 3000 mbsl (i.e., in the sediments of the abyssal plain) (Claypool and Kaplan, 1974). DSDP Site 174 indicated that the trench sediments are gas-charged (Claypool and Kaplan, 1974), although the absence of a BSR in the abyssal plain or in the uplifted sediments of the first accretionary ridge suggests that the methane content of the trench sediments is below saturation in central Cascadia. This contrasts with southern Cascadia, where a BSR is observed to extend into the abyssal plain (Gulick et al., 1998), and with northern Cascadia, where gas hydrate is present in the first accretionary ridge (Expedition 311 Scientists, 2006). For a more general review of the multiple factors, including solubility, that affect gas hydrate stability in marine sediments, see Tréhu et al. (in press).

Differences have been documented in the composition of the clay fraction between the early Pleistocene to Holocene sediments that comprise the slope-basin deposits and the late Pliocene to early Pleistocene strata from the slope-basin deposits (**Underwood and Torres,** this volume; **Gràcia et al.,** this volume). The slope basin sediments contain, on average, 29% smectite, 31% illite, and 40% chlorite (+ kaolinite), whereas the late Pliocene to early Pleistocene strata from the underlying accretionary prism contain moderately greater amounts of smectite, with average values of 38% smectite, 27% illite, and 35% chlorite (+ kaolinite). The moderate enrichment of expandable clay minerals in the accreted sediments is likely due to detrital point sources associated with the ancestral Columbia River, combined with south-directed transport of hemipelagic suspensions and turbidity currents on the floor of Cascadia Basin (**Underwood and Torres,** this volume).

DYNAMIC EFFECTS LEADING TO HETEROGENEOUS GAS HYDRATE DISTRIBUTION

Estimates of average gas hydrate content (Milkov et al., 2003) mask the great heterogeneity in gas hydrate distribution at SHR (Tréhu et al., 2004b). This heterogeneity results from a variety of processes. Foremost is that two fundamentally different regimes operate to generate the gas hydrate deposits. Both regimes may operate simultaneously in any given locality. Throughout the region, some of the gas hydrate forms from methane generated in the upper few 100 m of sediment by microbial remobilization of organic carbon. Superimposed on this reaction-dominated regime is a transport-dominated regime in which methane is focused from a large volume of deeply buried sediment into a conduit

that feeds methane into the GHSZ to form rich gas hydrated deposits near the structural summit. These two regimes correspond to the more general distributed low-flux and focused high-flux regimes discussed by Tréhu et al. (in press).

Modulating the gas hydrate distribution, especially within the reaction-dominated regime, is the effect of lithology. Gas hydrate forms preferentially in relatively coarse grained sediments (Weinberger et al., 2005; **Su et al.,** this volume; **Gràcia et al.,** this volume), leading to large vertical variations in gas hydrate on the scale of centimeters. Borehole logging data have been used to further characterize azimuthal variability, which can range from 0% to 90% of the pore space at a given depth (Janik et al., 2003).

Reaction-Dominated Regime (Distributed Low Flux)

The methane in the cored sediments recovered from northern flank of the summit (Sites 1244–1247) and from the slope basin (Sites 1251 and 1252), was generated by microbial methanogenesis (**Claypool et al.,** this volume). At these sites, the relative rates of alkalinity production and removal are such that the onset of methanogenesis is clearly observed as a change in slope in the alkalinity profiles (Tréhu, Bohrmann, Rack, Torres, et al., 2003).

Measured alkalinity at any depth beneath the zone of sulfate reduction results from total dissolved inorganic carbon (DIC) addition by organic matter oxidation minus DIC removal as methane and authigenic carbonate. Alkalinity production due to organic matter oxidation can be calculated and extrapolated from the observed sulfate gradient (**Borowski,** this volume; **Claypool et al.,** this volume). The difference between the projected and observed alkalinity is a measure of the amount of DIC removed to form methane and authigenic carbonate (Fig. **F4A**). Methane production rates estimated with this approach are on the order of 10 mmol/m^3/yr in sediments just beneath the sulfate reduction zone and rapidly decrease to rates of <0.1 mmol/m^3/yr at depths greater than 100 mbsf (Fig. **F4B**). These rates are comparable to those found in other high-productivity continental margin settings and lead to methane supersaturation at of 30–50 mbsf, which corresponds to the observed onset of gas hydrate in the sediments at most Leg 204 sites (**Claypool et al.,** this volume). Within the gas hydrate stability zone, the hydrocarbon composition (C_1/C_2 > 10,000) and isotopic data ($\delta^{13}C_{CH4}$ of –65‰ to –77‰) are consistent with an in situ microbial source for the methane (Fig. **F4C**). The gas hydrate at these sites is, therefore, referred to as reaction dominated (**Claypool et al.,** this volume).

The carbon isotope and hydrocarbon observations (Fig. **F4**) are consistent with an observed increase in dissolved iodide and bromide concentrations (**Fehn et al.,** this volume), as these halogens are released into the pore fluids during marine organic matter diagenesis. The general observations for halogen concentrations are in good agreement with those found for other gas hydrate locations (e.g., Peru margin, Martin et al., 1993; Blake Ridge, Egeberg and Dickens, 1999; Nankai Trough, Fehn et al., 2003). However, age estimates based on ^{129}I measurements suggest that the iodine and methane in the pore waters sampled at Hydrate Ridge is older than 15 Ma, indicating fluid migration from early Eocene sources (**Fehn et al.,** this volume). Although sediments of that age do occur ~40 km to the east, these old ages are not

F4. Methane concentrations, production rates, and composition, p. 29.

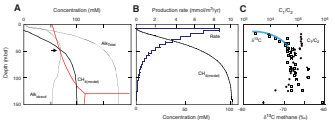

consistent with other geochemical data that indicate in situ methane generation. The reason for this discrepancy remains unresolved.

Transport-Dominated Regime (Focused High Flux)

The transport-dominated regime is associated with active venting of gas at the SHR summit (Sites 1248–1250), where gas seepage supports rapid growth of gas hydrates near the seafloor and vigorous anaerobic methane oxidation (Torres et al., 2002; Boetius et al., 2000; Boetius and Suess, 2004). Geophysical, geochemical, and lithologic data all indicate that Horizon A acts as a conduit delivering gas that has migrated from greater depth in the accretionary complex to the summit vents. Horizon A can be mapped as continuous surface that laps onto the accretionary complex to the east and intersects the BSR on the west. Updip from Site 1245, its amplitude is anomalously large (Fig. **F5A**). LWD density logs and shipboard porosity and grain density measurements can be used to calculate the free gas content of the pore space (Tréhu et al., 2004a) and indicate gas saturation high enough (50%–90%) to support a connected gas column that extends from at least the depth of Horizon A at Site 1245 to the summit. Assuming that the gas pressure at Site 1245 is equal to the hydrostatic pressure, gas pressure at the BSR beneath the summit may exceed lithostatic pressure, a condition that is compatible with migration of gas through fracturing of the overlying sediments (Fig. **F5B, F5C**). Coring at Sites 1245, 1247, 1248, and 1250 clearly indicated the anomalous nature of this 2- to 4-m-thick, volcanic ash–rich horizon, as illustrated by the in situ bulk density and grain size distribution at Site 1245 (Fig. **F5D**). We speculate that the overpressures evolved as gas hydrate formed where Horizon A entered the GHSZ, thus sealing this boundary and focusing gas toward the summit. Sampling of Horizon A within the GHSZ (which was not done during Leg 204 because of time constraints) is needed to test this hypothesis.

The gas geochemistry also supports the mechanical scenario indicated by geophysical and lithologic data. Horizon A shows the signature of migrated gas at all sites (i.e., relatively low C_1/C_2 and high $\delta^{13}C$) at which it was sampled (Fig. **F5E, F5F**), as do the shallow gas hydrates at the summit (Fig. **F5F**). Using the isotopic and chemical composition of gas samples, **Claypool et al.** (this volume) argue that the migrated gas component includes both previously buried microbial methane (~65% of the total gas) as well as thermogenic hydrocarbons (10%–15%). The isotopic composition of the thermogenic gas suggests an origin at temperatures in the range of 125°–135°C, or depths of 2.0–2.3 km (**Claypool et al.,** this volume **Tréhu,** this volume). This temperature is attained in underplated, duplexed, and accreted sediments (Fig. **F3B**). Seismic velocities obtained from vertical seismic profiles (**Tréhu et al.,** this volume) and sonic logs (**Guerin et al.,** this volume) provide further support for a gas-charged conduit (Fig. **F5G**). Low in situ *P*-wave velocity indicates abundant gas in the pore space. Low *S*-wave velocity suggests gas pressure high enough to result in a decrease in sediment shear strength and/or increase in pore space.

Although there is a consensus that Horizon A is the primary conduit feeding the summit vents and gas hydrate deposits, the mechanism whereby the gas migrates from Horizon A to and through the GHSZ remains controversial. Based on a one-dimensional, nonsteady-state transport reaction model, Torres et al. (2004b) argue that abundant

F5. Horizon A properties, p. 30.

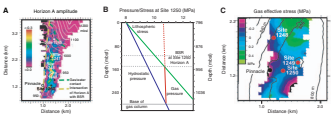

methane in the free gas phase must be supplied from below in order to reproduce the dissolved chloride and gas hydrate distributions observed at the ridge summit (Fig. **F5H**). They reproduce the observed Cl^- concentration and gas hydrate saturation by assuming vertical variation in the kinetic constants controlling methane dissolution and gas hydrate nucleation. Comparison of the internal pressures of gas hydrate crystallite and gas bubbles to the effective stress indicates that the depth at which gas hydrate can form by pushing away sediment grains corresponds approximately to the depth at the base of the shallow gas hydrate deposit (Fig. **F5H**). They conclude that capillary effects inhibit hydrate formation below ~30 mbsf, allowing methane gas to coexist with gas hydrate within the thermodynamically defined GHSZ (Clennell et al., 1999) and that gas migrates toward the ridge summit through a temporally variable network of pathways (Fig. **F5I**) controlled by catenary transport and/or pressure-dependent flow within hydrofractures (Tréhu et al., 2004a; Weinberger and Brown, 2006).

In contrast, based on the observations of high Cl^- concentration at shallow depth (Fig. **F5H**), which suggest that free gas may locally be in thermodynamic equilibrium (Milkov et al., 2004b), Milkov et al. (2005) and Liu and Flemings (2006) have argued that formation of gas hydrate where Horizon A enters the GHSZ led to formation of high-salinity pore fluid near the base of the GHSZ, which shifted the hydrate stability field sufficiently to preclude further gas hydrate formation. In this steady-state model, free gas migrates vertically beneath the carbonate pinnacle that overlies the intersection of Horizon A and the BSR and then is deflected laterally at ~30 mbsf to emerge at the seafloor in the summit bubble vents (Fig. **F5I**). Torres et al. (2005) discuss the evidence for and against these two models for moving gas through the GHSZ and conclude that both models are plausible and that neither model can be excluded at the present time.

Transport of methane dissolved in pore water appears to be a secondary process at the summit. Whereas lithium concentration and isotopic data suggest some migration of water along Horizon A (Tréhu, Bohrmann, Rack, Torres, et al., 2003; L.-H. Chan and M.E. Torres, pers. comm., 2006), boron and strontium isotope data (Teichert et al., 2005b) are inconclusive. In contrast, strontium, boron, and lithium concentration and isotope data suggest that the deep fluid is transported along Horizon B, sampled at Site 1244 (Teichert et al., 2005b) Drilling confirmed that Horizon B (Fig. **F2**) results from a 10-m-thick zone of multiple turbidites that contain some minor free gas below the GHSZ (Site 1244) (**Tréhu et al.,** this volume; **Guerin et al.,** this volume) and gas hydrate within the GHSZ (Site 1246). Unlike Horizon A, Horizons B and B′ do not appear to contain enough free gas at present to develop high gas pressure and drive free gas migration through the GHSZ and may represent a fluid regime intermediate between the focused and diffuse flow end-members. Where Horizon B and B′ were sampled within the GHSZ (at Site 1246), they contained more hydrate than adjacent fine-grained sediments, illustrating the modulating effect of lithology on gas hydrate distribution (see **"Lithologic Effects,"** below).

Lithologic Effects

Fine-scale distribution of gas hydrate varies strongly with depth over distances of centimeters, with gas hydrate present in lenses and nodules of submillimeter to centimeter thickness. These lenses and nodules are heterogeneously distributed, occurring in clusters that are several

meters thick and having orientations that range from horizontal to vertical (Tréhu et al., 2004b; Janik et al., 2003; **Abegg et al.,** this volume, submitted [**N1**]). A statistical correlation between grain size and hydrate content as inferred from infrared temperature anomalies indicates that turbidite deposits containing more silt and sand than the intervening hemipelagic deposits are preferential sites for gas hydrate formation (Weinberger et al., 2005; **Su et al.,** this volume). Similar lithologic overprinting of the gas hydrate distribution predicted by controls on gas hydrate distribution have been documented at Blake Ridge (Kraemer et al., 2000; Ginsberg et al., 2000), although the effect is not as strong because of the generally more homogeneous character of the Blake Ridge sediments. Comparison of results from Leg 204 to those from Expedition 311 (Expedition 311 Scientists, 2006), where numerous sand-rich horizons associated with gas hydrate were studied in detail, will further refine our understanding of the factors that control microscopic properties of gas hydrate growth.

One such cluster of gas hydrate lenses is associated with Horizon B (Fig. **F2B**) at Site 1246 (Fig. **F6**). Two coarse-grained turbidites characterized by high density and high magnetic susceptibility were found at 54–56.5 and 63.5–67 mbsf. These two horizons result in a strong, "ringy" reflection. The base of each turbidite was associated with cold infrared (IR) temperature anomalies; the lower one was also sampled for pore water analysis and yielded low pore water chloride indicative of 22% gas hydrate in the pore space, similar to the estimate of 28% gas hydrate determined from the IR data. At present, Horizon B is broken into many discontinuous segments because of normal faulting that is characteristic of the eastern flank of Hydrate Ridge. Because of evidence for free gas in Horizon B at Site 1244 and because of geochemical evidence for migration of fluids from greater depth, we speculate that Horizon B may have acted as an important conduit for free gas migration and may have fed a former seafloor vent system prior to being tectonically disrupted. Alternatively, the vertical faults in this region may facilitate upward fluid flow of fluids supersaturated with methane, which release this methane to form hydrate when they intersect Horizon B because the grain size and pore structure facilitate gas hydrate nucleation.

F6. Nested view of data from Horizon B in Hole 1246B, p. 33.

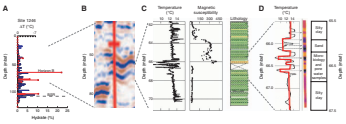

Lateral Heterogeneity at the Base of Gas Hydrate Stability

Strong lateral heterogeneity in gas hydrate distribution near the base of the GHSZ is indicated by a comparison of results in several different holes, spaced 30–40 m apart, at Site 1251. At this site, the reflection strength of the BSR and of the underlying reflectivity, which is attributed to the presence of lithologically controlled free gas, vary over short distances (Fig. **F7A**). Resistivity and nuclear magnetic resonance (NMR) data from Hole 1251A were interpreted to indicate free gas below the BSR but were not interpreted to show gas hydrate just above the BSR (**Collett et al.,** this volume), although the resistivity data indicate that some gas hydrate is possible (Fig. **F7B**). In contrast, a 12-m-thick zone of relatively high gas hydrate content (~15% of pore space) was observed immediately above the BSR in Hole 1251D based on IR and chloride data (Fig. **F7C**). In Hole 1251H, the sonic log indicates gas hydrate enrichment of a few percent immediately above the BSR (**Guerin et al.,** this volume).

This basal hydrate-rich layer may be the result of recycling of methane released in response to upward migration of the base of the gas hy-

F7. Lateral variability among holes at the same site, p. 34.

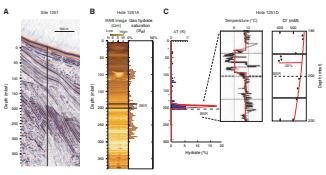

drate stability zone triggered by rapid deposition of the overlying slope basin sediments. Sediments presently above the BSR were deposited at a rate of 60–160 cm/k.y. (Tréhu, Bohrmann, Rack, Torres, et al., 2003). A sharp decrease at the BSR in the C_1/C_2 ratio of gas exsolved from pore water is consistent with this model (**Claypool et al.,** this volume). Although no significant variation in grain size in sediments associated with gas hydrate at this site has been documented, a more detailed look at variations in grain size and other lithologic parameters is warranted because the seismic data suggest that the distribution of free gas beneath the BSR is lithologically controlled. A similar concentration of gas hydrate just above the BSR may also be present at Site 1247. Such patchy lenses of anomalously high gas hydrate concentration at the base of the GHSZ have the potential to lead to deeply buried zones of high pore pressure and slope instability if these hydrates are destabilized as a result of tectonic uplift or a drop in sea level (Xu, 2004).

INTERCALIBRATION OF DIFFERENT GAS HYDRATE PROXIES

In the previous section, we discussed the impact of Leg 204 on our understanding of gas hydrate processes in an accretionary complex based on information on the gas hydrate distribution. In this section, we discuss the techniques whereby this gas hydrate distribution was determined. Because gas hydrate is not stable at the sea surface, these estimates are based on various proxies. Some of these (e.g., pressure cores and pore water Cl^- anomalies) provide well-constrained but incomplete estimates of the gas hydrate content of the subsurface because they sample only a small fraction of sediments within the GHSZ, whereas others (e.g., resistivity and sonic logs and infrared thermal anomalies) provide good spatial coverage, but algorithms for quantifying gas hydrate from the observations must be calibrated and verified by other techniques. Using data from Site 1244, Figure **F8** illustrates the variety of length scales to which these different data sets are sensitive. It also provides additional evidence for lateral heterogeneity between holes spaced tens of meters apart at a given site. Table **T2** shows that estimates of the average gas hydrate content of the sediments derived by different techniques are generally similar. It is also apparent that regions characterized by many faults, as imaged by the seismic data (e.g., Site 1244 and 1246), show more variability between holes at a particular site than regions characterized by simple structure (e.g., Site 1245).

Pressure Core Samplers

Pressure core samplers allow us to recover short (~1 m) sediment cores at in situ pressure conditions (Dickens et al., 1997). This is the only way to recover all in situ methane and thus directly measure the total gas concentration at discrete depths within sediment sequences. The gas hydrate content of the core can then be calculated from the total methane concentration assuming thermodynamic equilibrium and that porosity and pore water chemistry are known (Dickens et al., 2000).

A record-breaking number of pressure core samples for a single cruise was obtained during Leg 204. As the most direct measurement of gas hydrate content, results from these cores provide a good estimate of the average amount of gas hydrate present within the study region (Milkov

F8. Gamma density and IR image of a HYACINTH pressure core and Cl^- and RAB data, p. 35.

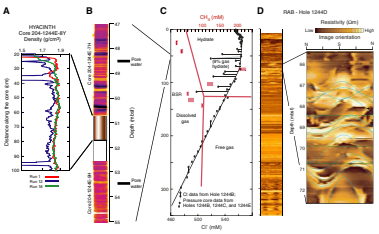

T2. Average hydrate contents, p. 38.

et al., 2003); they also provide critical information to test estimates of gas hydrate content obtained by other means (Tréhu et al., 2004b). In general, however, pressure core data provide limited constraint on the details of gas hydrate distribution because the number of pressure core samples at a given site is too few to define the vertical variation in gas hydrate content.

Leg 204 was a testbed for a new generation of pressure core samplers (the HYACE system), which was designed so that cores recovered under pressure can be logged at in situ conditions and as pressure is released (Fig. **F8A**). The HYACE cores provided critical information about how gas hydrate is distributed within cores at in situ conditions and how it responds as pressure is released (Tréhu, Bohrmann, Rack, Torres, et al., 2003; Tréhu et al., 2004b).

Infrared Camera Scans of Cores

Gas hydrate dissociation is strongly endothermic, resulting in cold spots in cores (Figs. **F6C, F6D, F7C, F8B**), which were originally detected by hand (e.g., Paull, Matsumoto, Wallace, et al., 1996). Infrared cameras were first introduced to ODP during Leg 201 (Ford et al., 2003) and were used systematically to scan all core recovered from within or near the GHSZ during Leg 204. These scans were invaluable for rapidly identifying gas hydrate samples for special shipboard experiments (e.g., Riedel et al., 2006) or for preservation in liquid nitrogen for future studies (e.g., **Abegg et al.,** this volume).

An important advantage of this technique, which distinguishes this approach from the continuous geophysical records obtained by downhole logging, is the ability to directly sample lithologies and pore waters associated with the IR anomalies. Initial attempts to calibrate the anomalies recorded in catwalk core scans using coincident measurements of chloride concentration were presented by Tréhu et al. (2004b). These data provide important information on the spatial distribution of gas hydrate, including the thickness, spacing, and shape of gas hydrate lenses and nodules (Weinberger et al., 2005). Although the amplitude of any particular anomaly depends on how the hydrate is distributed in the core, the average gas hydrate content of the sediments can be estimated using simple, empirical calibrations based on pore water Cl^- data (Tréhu et al., 2004b).

Geochemical Anomalies

The most widely used geochemical proxy for gas hydrate presence is based on the accurate measurement of dissolved chloride (Cl^-) in the pore fluids. During core recovery, gas hydrate dissociates, resulting in dilution of the Cl^- concentration by addition of water sequestered in the gas hydrate lattice prior to core recovery. The use of the Cl^- proxy is predicated on the assumption that the background Cl^- concentration is known and that the rate of hydrate formation is slow enough that high Cl^- anomalies resulting from salt exclusion during hydrate formation have been removed by diffusion and advection (Hesse and Harrison, 1981; Ussler and Paull, 2001). For example, in Figure **F8C,** different gas hydrate estimates are derived if the background Cl^- content of the pore water is assumed to be equal to that of seawater or if only the discrete low Cl^- spike is attributed to gas hydrate dissociation (i.e., using an empirical baseline). With the latter assumption, the maximum gas hydrate

content indicated by Cl^- data at Site 1244 is ~8% of the pore space and the average gas hydrate content of the gas hydrate–bearing sediment that extends from 30 to 130 mbsf is ~3% (Tréhu et al., 2004b). Increased freshening of pore waters with subseafloor depth and with distance from the deformation front at Sites 1244–1246, 1251, and 1252 (Fig. F2A) has been used to separate effects of clay dehydration reactions and gas hydrate dissociation on the dissolved Cl^- distribution (Torres et al., 2004a). The observations are consistent with enhanced conversion of smectite to illite, driven by an increase in temperature and age of the accreted sediments. The gas hydrate pore space saturations derived from Cl^- data in Figures F6 and F7 were also determined using an empirical baseline.

Compared to PCS samples, more chloride samples are obtained in each hole and each sample averages over a smaller distance; nonetheless, considerable statistical undersampling remains. Another important use of chloride data during Leg 204 was to calibrate data from IR temperature scans (see "Infrared Camera Scans of Cores," p. 11). This line of inquiry was further developed during IODP Expedition 311 (Expedition 311 Scientists, 2005). One limitation of Cl^- as a gas hydrate proxy during Leg 204 was that it cannot be used when hydrate is forming more rapidly than the excluded salts can be removed by diffusion or fluid advection. This was the case in the shallow subsurface near the summit (Fig. F5H). However, in this case, the resultant brines provide important constraints on system dynamics, as discussed in "Transport-Dominated Regime," p. 7. There may also be problems defining a baseline when gas hydrate is evenly disseminated in the pore space over tens of meters in depth.

A possible new geochemical proxy is discussed by Milkov et al. (2004a). Ethane-enriched Structure I gas hydrate solids are buried more rapidly than ethane-depleted dissolved gas in the pore water because of upward advection of pore water due to compaction. With subsidence beneath the GHSZ, the ethane (mainly of low-temperature thermogenic origin) is released back to the dissolved gas–free gas phases and produces a discontinuous decrease in the C_1/C_2 vs. depth trend. These ethane fractionation effects may also be useful to reconstruct upward migration of the base of the gas hydrate stability field in the past (Claypool et al., this volume). For example, release of ethane from gas hydrate may be responsible for the increase in ethane in pore waters from beneath the BSR at Site 1251.

Downhole Geophysical Logs

Various downhole geophysical logs were used to estimate the gas hydrate content of the subsurface, including electrical resistivity (Tréhu, Bohrmann, Rack, Torres, et al., 2003; Lee and Collett, this volume; Janik et al., 2003), sonic velocity (Lee and Collett, this volume; Guerin et al., this volume), and NMR (Collett et al., this volume), and were critical for determining the gas saturation in Horizon A (see "Transport-Dominated Regime," p. 7).

Geophysical logs provide a number of important advantages: (1) they are relatively quick and economical to acquire; (2) they provide nearly continuous coverage of the subsurface, except for in the upper few tens of meters where log quality is bad (e.g., Figs. F5D, F7B, F8D); (3) they image the subsurface with the highest resolution, with some techniques providing centimeter-scale azimuthal images of the bore-

hole (e.g., Fig. F8D); and (4) they provide unique information on in situ physical properties (e.g., density, electrical resistivity, seismic velocity, and in situ stress), which cannot be measured on core samples because of degassing and deformation during core recovery (e.g., Fig. F5D, F5G).

However, a number of assumptions are needed to derive estimates of the gas hydrate content of the sediments from geophysical logs, and it is difficult to directly test the validity of these assumptions, particularly when no core data are available from a logged hole, as is the case with most LWD data and when core recovery is poor. For example, electrical resistivity data cannot distinguish between gas hydrate and free gas. Comparisons between different holes that are several tens of meters apart are difficult because it is clear that there is considerable lateral heterogeneity in gas hydrate distribution (see "Lateral Heterogeneity in Gas Hydrate Content," p. 9).

Seismic Experiments

Seismic data acquired during Leg 204, including vertical, offset, and walkaway VSPs and regional high-resolution seismic reflection and refraction profiles, provide the largest-scale estimates of gas hydrate distribution. Successful VSPs were acquired at Sites 1244, 1247, and 1250 (Tréhu et al., this volume; Guerin et al., this volume). These data indicate that, in contrast to results from Legs 146 and 164 where free gas is present in a zone tens to hundreds of meters thick beneath the BSR (e.g., MacKay et al., 1994; Holbrook et al., 1996), free gas beneath the GHSZ at SHR is restricted to narrow, stratigraphically controlled conduits (e.g., Fig. F5G). Walkaway VSPs and regional ocean bottom seismograph (OBS) refraction profiles, which indicate velocity anisotropy beneath the summit but not beneath the adjacent basin, help to characterize gas hydrate distribution away from the drill sites. These data suggest that gas hydrate near the base of the GHSZ in the summit region is concentrated in vertical fractures that are aligned along the ridge axis and does not significantly impact the stiffness of the sediment (Kumar et al., 2006, in press).

MECHANICAL AND HYDROLOGIC PROPERTIES OF CORED SEDIMENTS

Mechanical properties of the cored sediments are discussed in several papers. Riedel et al. (this volume) present data on a broad suite of physical properties measurements from the upper 10–20 mbsf. These results are important because of the poor quality of logs from these depths. Apparent overconsolidation of shallow sediments from the ridge (Sites 1244, 1245, and 1246) and normal consolidation in the slope basin (Sites 1251 and 1252) supports the inference from seismic stratigraphic analysis that the ridge is presently an erosional environment.

Tan et al. (this volume) present results of consolidation tests on whole-round samples from Site 1244, which provide important background information for future hydrological analyses. Winters et al. (this volume) present results of consolidation tests on a sample from the summit region that was thought to have contained gas hydrate, based on an IR anomaly recorded on board. This sample was repressurized to in situ pressure immediately after recovery; however, no gas hy-

drate was observed when the sample was removed from the pressure vessel for mechanical tests.

Borehole breakouts observed in the electrical resistivity logs provide unique information on the orientation of the present stress field at SHR and on the in situ mechanical properties of gas hydrate–bearing sediments (**Goldberg and Janik,** this volume). At Sites 1244 and 1245, the stress direction is dominated by the topographic effect of SHR, whereas at Site 1251, in the slope basin, the stress direction is approximately perpendicular to the plate convergence direction. Except at the summit, which is characterized by chaotic fracturing indicative of free gas migration, the orientations of resistive fractures, also imaged by the resistivity logs, are consistent with these stress directions (Weinberger and Brown, 2006).

GAS HYDRATE STRUCTURE AND FABRIC

During Leg 204, numerous gas hydrate samples, as detected by IR imaging on the catwalk, were recovered as whole rounds and preserved in liquid nitrogen for detailed shore-based studies. Unfortunately, the preservation status of such hydrates was compromised somewhat because of gas hydrate decomposition during recovery, which apparently continued while the samples were still cooling after their submergence in liquid nitrogen.

X-ray diffraction (XRD) analyses on gas hydrate samples preserved in liquid nitrogen document that only Structure I hydrate is present (Kim et al., 2005; Bohrmann et al., in press), confirming conclusions from gas analyses of distinct hydrate samples (Milkov et al., 2005). XRD measurements using synchroton radiation and Rietveld analyses allowed a quantitative estimate of the preservation status of these hydrate samples (Bohrmann et al., in press). Out of 13 distinct samples from various depths at Sites 1244, 1245, and 1247–1250, 8 samples contained 1%–7% hydrate and >90% ice. The ice probably represents water from dissociated hydrate (Bohrmann et al., in press). Five samples showed higher gas hydrate amounts of 20%–70% and lower concentrations of ice (30%–75%), with other mineral phases (e.g., quartz) comprising up to 8% of the sample. Bohrmann et al. (in press) have recognized a correlation between the volume of gas hydrate originally present in the host sediment and the degree of preservation of the gas hydrate samples.

Abegg et al. (this volume, submitted [**N1**]) investigated a total of 65 frozen whole-round samples from six sites using X-ray computerized tomographic (CT) imaging. Although most of the whole-round samples stored in liquid nitrogen showed widespread decomposition of gas hydrate, the original presence of gas hydrate in the sediment cores was indicated by low-density anomalies. In many cases the gas hydrate itself was no longer present and had been replaced by a distinctive fabric that reflects the frozen state of a soupy sediment full of bubbles. Detailed fabric analyses of the samples showed that the hydrates had been present in layers with a variety of dips. Shallow hydrate layers parallel or subparallel to bedding are interpreted to result from gas bubble injections parallel to the layering of sedimentary deposits. Deeper than 40 mbsf, hydrate layers are characterized by steeper dip angles of 30°–90° and are interpreted as precipitates in open fractures or joints, consistent with a model in which free gas migrates through the sediments by opening cracks, which close as gas hydrate is precipitated, leading to formation of new cracks (Weinberger and Brown, 2006).

Isotopic data also suggest structural differences between gas hydrate formed in a transport-dominated regime and gas hydrate formed in the reaction-dominated regime. Tomaru et al. (in press) show that the isotopic fractionation of the water in the lattice of the massive gas hydrate (α_O = 1.0010 and α_H = 1.008) is significantly lower than that observed in the disseminated, nodular, or vein-filling deposits (α_O = 1.0025 and α_H = 1.022). The authors suggest that the anomalous fractionation may be caused by lower gas occupancy in the massive deposits.

THERMAL REGIME OF SOUTHERN HYDRATE RIDGE

Heat flow data from Leg 204 are summarized in Table **T3.** Detailed discussion of data analysis and uncertainties is presented by **Tréhu** (this volume). The uncertainties in heat flow shown here include an estimated uncertainty of ±0.1 W/(m·K) in thermal conductivity, ±0.3°C in temperature, and ±2 km in depth. The data indicate that the thermal gradient is dominated by conduction and that the base of the GHSZ predicted by the thermal gradient and pore water composition is consistent with that indicated by seismic observations of BSR depth, although an offset of up to 15 m is allowable at several sites. Lack of curvature in the temperature vs. depth profiles indicates that heat transport through advection of pore fluid is below the thermal detection threshold of 1–10 cm/yr (Wang et al., 1993; Tréhu, Bohrmann, Rack, Torres, et al., 2003; Torres et al., 2004b). The apparent paradox of very low rates of fluid advection combined with observations of venting of gas bubbles, geochemical signatures of gas migration, and formation of abundant gas hydrate near the seafloor can be reconciled by models in which methane is transported through the sediments as free gas (e.g., Torres et al., 2004b; Milkov et al., 2005; Tréhu et al., 2004a; Liu and Flemings, 2006).

T3. Thermal gradients and heat flow, p. 39.

One of the striking results is the small variation in heat flow from site to site, including sites near the active vents near the summit of SHR as well as sites on the flanks and in the adjacent slope basin. The data are generally consistent with the model of Hyndman et al. (1993) and Wang et al. (1993), in which tectonically induced sediment thickening depresses the thermal gradient near the deformation front. This model predicts a thermal gradient in shallow sediments near the deformation front that is lower than the gradient predicted by a simple conductive model of a thick, sediment pile overlying young oceanic crust; farther landward, the thermal gradient will approach the gradient predicted by the conductive model as fluid is expelled from overpressured sediments. The thermal gradient can therefore be used to constrain large-scale fluid flow in the accretionary complex. At SHR, the apparent heat flow across the entire region studied during Leg 204 is only ~60% of that predicted by a conductive thermal model (Oleskevich et al., 1999). This suggests that fluid expulsion continues to the east beneath the mid and upper slope and continental shelf, consistent with observations of pockmarks and other vent structures in this region (e.g., Johnson et al., 2003).

Leg 204 also provided an opportunity to successfully test a new instrument that continuously recorded the temperature, pressure and electrical conductivity at the top of an APC core during the entire coring and core recovery process (**Ussler et al.,** this volume). The data have

the potential to lead to a better understanding of gas hydrate dissociation during core recovery.

SIGNS OF PAST GAS HYDRATE PRESENCE

One of the objectives of Leg 204 was to identify and calibrate proxies for the presence of gas hydrate in the past. Several studies addressed this issue. A second, fainter negative polarity reflection that is observed ~30 m beneath the western flank of SHR has been interpreted to result from gas trapped in impermeable sediments after shallowing of the BSR in response to ocean warming (Bangs et al., 2005). The presence of magnetic minerals that can be associated with gas hydrate supports this interpretation (Musgrave et al., 2006; **Larrasoaña et al.,** this volume). However, this observation is also compatible with the presence of a small amount of Structure II hydrate that contains higher-order hydrocarbons in the interval between the primary and secondary BSRs (**Claypool et al.,** this volume). Although no direct or indirect evidence for gas hydrate was found in this interval, gas chemistry allows the possibility of this alternative explanation.

Because carbonate deposits are closely associated with the history of methane discharge and of the processes that transform the carbon in methane to carbonate, these mineral phases contain valuable information to reconstruct the history and processes driving gas hydrate formation and dissociation. Isotopic analyses of carbonates from Leg 204 indicate that only carbonates sampled in Holes 1248B, 1249C, and 1249K are related to anaerobic methane oxidation, as reflected in their $\delta^{13}C$ values; most of the other carbonates sampled reflect a DIC source that originated from the remineralization of organic matter (B.M.A. Teichert, pers. comm., 2006).

In addition to documenting gas hydrate history, authigenic carbonate formation also alters pore water chemistry. Carbonate precipitation contributes to a decrease in the $\delta^{18}O$ of the pore water at all sites (**Tomaru et al.,** this volume); however, $\delta^{18}O$ is also affected by hydrate formation and decomposition, clay mineral dehydration, and alteration of oceanic crust, and separation of these effects requires further modeling. Authigenic carbonate precipitation and dissolution may also impact dissolved fluoride concentrations (**Dickens et al.,** this volume). However, because of a lack of data on the concentration of halogens in the various carbonate phases, this idea remains untested.

MICROBIOLOGY

A key contribution to the Leg 204 investigations was the characterization of various components of the carbon cycle, which allows inferences on microbial processes and activity rates in this region. In areas of active methane venting near the summit of SHR, microbiological (e.g., Boetius et al., 2000; Knittel et al., 2005) and isotopic (Torres et al., 2003; **Torres and Rugh,** this volume) data indicate that high anaerobic methane oxidation rates near the seafloor are supported by rapid methane flux. In contrast, at the sites drilled in slope basin and on the saddle north of the southern summit, anaerobic oxidation of methane is minor or absent, as indicated by the distribution of metabolites in the pore fluids and isotopic composition of the dissolved inorganic carbon (**Claypool et al.,** this volume; **Torres and Rugh,** this volume;

Borowski, this volume). At these sites, sulfate is consumed primarily by oxidation of organic matter, and sulfate reduction rates estimated from curve fitting of concentration gradients are in the range of 2–4 mmol/m^3/yr, with integrated net rates of 20–50 mmol/m^2/yr. Microbial methane production rates derived from the geochemical data are ~1.5 mmol/m^3/yr in sediments just beneath the sulfate reduction zone and decrease to <0.1 mmol/m^3/yr at depths greater than 100 mbsf. These rates overlap with, but are generally lower than, those obtained in laboratory incubations of samples from NHR, where methane was produced at ~0.9–9.0 mmol/m^3/yr (Cragg et al., 1996).

Using a method that involved enumeration of methanogens in nearly 50 Leg 204 samples combined with determinations of minimal rates of methane production obtained from lab reactors, Colwell et al. (2004) estimated that most of the samples measured (~75%) exhibited rates of <0.0016 mmol/m^3/yr and rare samples had rates estimated as high as 70 mmol/m^3/yr. Centimeter-scale investigations of the geological or geochemical conditions that determine how rapidly methanogens make methane in Hydrate Ridge sediments were not attempted as a part of this research; however, such studies would advance our understanding of the abiotic controls that determine how methanogenic rates can apparently range over several orders of magnitude in closely spaced samples. Other research in deep marine sediments has found that geological and geochemical characteristics determine the rates for key biogeochemical processes (D'Hondt et al., 2004; Parkes et al., 2005). A study of the distribution of acetate and hydrogen, two key methanogenic electron donors, performed on Leg 204 sediments indicated that these sources of energy are present in relatively high concentrations (3.17–2515 M) and show intriguing peaks at some depths in the sediments (Lorenson et al., this volume); for example, acetate maxima and localized high acetate concentrations occurred at the BSR at all sites and frequently corresponded with areas of gas hydrate accumulation.

In order to evaluate whether the presence of gas hydrates has bearing on the biogeographical distribution and phylogenetic diversity of microbial communities present in seafloor sediments, microbial deoxyribonucleic acid (DNA) was extracted from samples collected as a part of Leg 204 and then amplified using universal primers that target 16S ribosomal ribonucleic acid (rRNA) genes. The resulting Leg 204 clone libraries were used together with similar libraries constructed from Leg 201 samples. The analysis of this extraordinarily large collection of clone sequences demonstrated that for the tested sediments the presence of hydrates corresponded to microbial communities that were statistically distinct from the communities that were present in sediments lacking hydrates (Inagaki et al., 2006). Notably, the as-yet-uncultivated Archaea of the Deep Sea Archaeal Group, and the Bacteria of the JS1 Group, Planctomycetes, and the Chloroflexi, were important members of hydrate-bearing sediments, but they were less apparent in nonhydrate-bearing sediments. As in a number of prior investigations that sought the presence of methanogenic Archaea in hydrate-bearing sediments, these methane-producing cells were not detected in the clone libraries. However, when the methanogenic functional gene for methyl coenzyme M reductase (*mcr*) was targeted in quantitative polymerase chain reaction experiments, ~25% of the Leg 204 samples showed evidence of detectable levels of this gene, suggesting the presence of these cells, albeit at low levels (Colwell et al., 2004). These studies augment past investigations of the Cascadia margin sediments, which found that meth-

anogen diversity was low, with all of the detected sequences associated with the Methanosarcinales and Methanobacteriales groups (Marchesi et al., 2001).

To further address the metabolic capability of microorganisms in this methane-rich deep biosphere environment, the stable carbon isotopic compositions of intact polar lipids, derived from live cells in the samples, were correlated with microbial diversity and activity measurements in discrete samples (B. Orcutt, pers. comm., 2006; Orcutt, 2006). In near-surface samples from the summit of SHR, where massive gas hydrate is supported by upward methane advection, highly depleted derivatives of archaeal and bacterial lipids indicate the incorporation of methane-derived carbon into microbial biomass, presumably by members of the ANME-1 clade. Samples collected below zones of massive hydrate at the summit sites contain both Archaea and Bacteria in varying proportions as evidenced by lipid biomarker and 16S rDNA based tools. Archaea of the Deep Sea Archaeal Group of Crenarchaea were detected in all subsurface samples analyzed, and the ANME-1 group of Euryarchaea, together with sulfate-reducing bacteria, were detected in the deep subsurface (54 mbsf) for the first time. However, archaeal and bacterial lipids derived from these samples show that these microorganisms are not substantially depleted in ^{13}C, as known from other microbial habitats dominated by anaerobic oxidation of methane. It is possible that environmental factors such as sulfate depletion limit the distribution, activity, and growth of anaerobic methanotrophs in the deep subsurface. In combination with previous investigations (Biddle et al., 2006), these results may also indicate that the low diversity of Archaea in the deep biosphere cycle methane in a manner that is biochemically different from methane consumers in the near surface, likely due to the constraint of energy limitation in the deep biosphere.

CONCLUSION

Leg 204 demonstrated the need for a multidisciplinary "hydrocarbon systems" approach toward modeling, integrating, and interpreting a wide range of geological, biogeochemical, and geophysical data in order to understand the formation and evolution of marine gas hydrate deposits and to predict gas hydrate distribution elsewhere. Geophysical and geochemical analyses provide complementary data for understanding the source of gas for gas hydrate formation and the mechanisms whereby it migrates into the GHSZ. Two fundamentally different gas delivery processes coexist in the region of southern Hydrate Ridge to generate the observed gas hydrate distribution. The rich gas hydrate deposit observed near the seafloor at the summit, which contains ~30% gas hydrate by volume and extends to a depth of 20–30 mbsf, results from migration and focusing of methane by geologic structure. At south Hydrate Ridge, the structure that acts as a gas conduit is a 2- to 4-cm-thick volcanic ash–rich layer that is surrounded by less permeable sediments and has been folded to form an anticline. Modeling suggests that an abundant supply of free gas is needed to generate the massive gas hydrates and high-Cl^- pore waters observed at the summit. Throughout the region, gas hydrate, which occupies, on average, 2%–8% of the pore space, is present in a depth range that extends from ~30 mbsf to the BSR. The distribution of gas hydrate within this zone is very heterogeneous, both vertically and horizontally. The amount of gas hydrate and whether it fills pore space or forms steeply dipping veins and

subhorizontal lenses is determined by a variety of factors, including the rate of microbial methane production, the rate of diffuse fluid flow, lithology, and faulting, with gas hydrate forming preferentially in relatively coarse grained or faulted strata.

Although Leg 204 greatly improved our understanding of gas hydrate processes in accretionary complexes, a number of important questions remain unanswered. Here we give a few examples. (1) The mechanism whereby gas migrates through the gas hydrate stability zone to form shallow, massive gas hydrate or vent into the ocean and the rate at which this occurs remain poorly controlled. In situ time-series observations on and below the seafloor are needed. (2) Questions also remain about the generality of some of the empirical relationships used to convert geophysical observations to in situ gas hydrate quantity. Much of the apparent variability in gas hydrate content derived using different techniques in neighboring holes is likely due to actual heterogeneity in the gas hydrate distribution, although some may be due to uncertainties in the calibration of various gas hydrate proxies. Separating these effects will require acquisition of new data sets from a variety of geologic settings in which multiple proxies are available from the same hole, as well as additional detailed analysis of existing data sets. (3) A better understanding of the response of submarine gas hydrates to oceanographic and tectonic perturbations and resulting temporal variations in the supply of methane require new models that incorporate the heterogeneity found in natural systems. (4) Ambiguity remains about whether a second faint BSR located ~30 m below the current base of the GHSZ is due to the presence of Structure II hydrate or is a relic from a time when the BSR was deeper. (5) Factors controlling the relative roles of microbial oxidation of organic carbon and anaerobic oxidation of methane, in particular the possible existence of threshold metabolite levels in controlling microbial activity and the role of fluid flow in supplying such metabolites, need to be determined through improved microbial sampling and culturing techniques and integration of biological, geochemical, and geophysical data and models.

ACKNOWLEDGMENTS

This research used samples and/or data provided by the Ocean Drilling Program (ODP). ODP is sponsored by the U.S. National Science Foundation and participating countries under management of Joint Oceanographic Institutions (JOI), Inc. An earlier version of the manuscript benefitted from reviews by C.K. Paull and an anonymous reviewer.

REFERENCES

Bangs, N.L.B., Musgrave, R.J., and Tréhu, A.M., 2005. Upward shifts in the southern Hydrate Ridge gas hydrate zone following postglacial warming, offshore Oregon. *J. Geophys. Res.,* 110(B3):B03102. **doi:10.1029/2004JB003293**

Biddle, J.F., Lipp, J.S., Lever, M., Lloyd, K., Sørensen, K., Anderson, R., Fredricks, H.F., Elvert, M., Kelly, T.J., Schrag, D.P., Sogin, M.L., Brenchley, J.E., Teske, A., House, C.H., and Hinrichs, K.-U., 2006. Heterotrophic archaea dominate sedimentary subsurface ecosystems off Peru. *Proc. Natl. Acad. Sci. U. S. A.,* 103(10):3846–3851. **doi:10.1073/pnas.0600035103**

Boetius, A., Ravenschlag, K., Schubert, C.J., Rickert, D., Widdel, F., Gieseke, A., Amann, R., Jørgensen, B.B., Witte, U., and Pfannkuche, O., 2000. A marine microbial consortium apparently mediating anaerobic oxidation of methane. *Nature (London, U. K.),* 407:623–626. **doi:10.1038/35036572**

Boetius, A., and Suess, E., 2004. Hydrate Ridge: a natural laboratory for the study of microbial life fueled by methane from near surface gas hydrates. *Chem. Geol.,* 205(3–4):291–310. **doi:10.1016/j.chemgeo.2003.12.034**

Bohrmann, G., Greinert, J., Suess, E., and Torres, M., 1998. Authigenic carbonates from the Cascadia subduction zone and their relation to gas hydrate stability. *Geology,* 26(7):647–650. **doi:10.1130/0091-7613(1998)026<0647:ACFTCS>2.3.CO;2**

Bohrmann, G., Kuhs, W.F., Staykova, D.K., Techmer, K., Klein, H., Murshed, M., and Abegg, F., in press. Appearance and preservation of natural gas hydrate from Hydrate Ridge sampled during ODP Leg 204 drilling. *Mar. Geol.*

Claypool, G.E., and Kaplan, I.R., 1974. The origin and distribution of methane in marine sediments. *In* Kaplan, I.R. (Ed.), *Natural Gases in Marine Sediments:* New York (Plenum), 99–139.

Clennell, M.B., Hovland, M., Booth, J.S., Henry, P., and Winters, W.J., 1999. Formation of natural gas hydrates in marine sediments. 1. Conceptual model of gas hydrate growth conditioned by host sediment properties. *J. Geophys. Res.,* 104(B10):22985–23004. **doi:10.1029/1999JB900175**

Colwell, F.S., Boyd, S., Delwiche, M.E., and Reed, D.R., 2004. Realistic rates of biological methane production in hydrate bearing sediments [presented at the AAPG Hedberg Research Conference, 12–16 September 2004, Vancouver, B.C.].

Cragg, B.A., Parkes, R.J., Fry, J.C., Weightman, A.J., Rochelle, P.A., and Maxwell, J.R., 1996. Bacterial populations and processes in sediments containing gas hydrates (ODP Leg 146: Cascadia Margin). *Earth Planet. Sci. Lett.,* 139(3–4):497–507. **doi:10.1016/0012-821X(95)00246-9**

D'Hondt, S., Jørgensen, B.B., Miller, D.J., Batzke, A., Blake, R., Cragg, B.A., Cypionka, H., Dickens, G.R., Ferdelman, T., Hinrichs, K.-U., Holm, N.G., Mitterrer, R., Spivack, A., Wang, G., Bekins, B., Engelen, B., Ford, K., Gettemy, G., Rutherford, S.D., Sass, H., Skilbeck, C.G., Aiello, I.W., Guèrin, G., House, C.H., Inagaki, F., Meister, P., Naehr, T., Niitsuma, S., Parkes, R.J., Schippers, A., Smith, D.C., Teske, A., Wiegel, J., Naranjo Padilla, C., and Acosta, J.L.S., 2004. Distributions of microbial activities in deep subseafloor sediments. *Science,* 306(5705):2216–2221. **doi:10.1126/science.1101155**

Dickens, G.R., Paull, C.K., and Wallace, P., 1997. Direct measurement of in situ methane quantities in a large gas-hydrate reservoir. *Nature (London, U. K.),* 385(6615):426–428. **doi:10.1038/385426a0**

Dickens, G.R., Wallace, P.J., Paull, C.K., and Borowski, W.S., 2000. Detection of methane gas hydrate in the pressure core sampler (PCS): volume-pressure-time relations during controlled degassing experiments. *In* Paull, C.K., Matsumoto, R., Wallace, P.J., and Dillon, W.P. (Eds.), *Proc. ODP, Sci. Results,* 164: College Station, TX (Ocean Drilling Program), 113–126. **doi:10.2973/odp.proc.sr.164.210.2000**

Egeberg, P.K., and Dickens, G.R., 1999. Thermodynamic and pore water halogen constraints on gas hydrate distribution at ODP Site 997 (Blake Ridge). *Chem. Geol.,* 153:53–79.

Expedition 311 Scientists, 2005. Cascadia margin gas hydrates. *IODP Prel. Rept.,* 311. **doi:10.2204/iodp.pr.311.2005**

Expedition 311 Scientists, 2006. Expedition 311 summary. *In* Riedel, M., Collett, T.S., Malone, M.J., and the Expedition 311 Scientists. *Proc. IODP,* 311: Washington, DC (Integrated Ocean Drilling Program Management International, Inc.). **doi:10.2204/iodp.proc.311.101.2006**

Expedition 311 Scientists, 2006. Site U1326. *In* Riedel, M., Collett, T.S., Malone, M.J., and the Expedition 311 Scientists. *Proc. IODP,* 311: Washington, DC (Integrated Ocean Drilling Program Management International, Inc.). **doi:10.2204/iodp.proc.311.104.2006**

Fehn, U., Snyder, G.T., Matsumoto, R., Muramamtmsu, Y., and Tomaru, H., 2003. Iodine dating of pore waters associated with gas hydrates in the Nankai area, Japan. *Geology,* 31:521–524.

Fisher, M.A., Flueh, E.R., Scholl, D.W., Parsons, T., Wells, R.E., Tréhu, A.M., ten Brink, U., and Weaver, C.S., 1999. Geologic processes of accretion in the Cascadia subduction zone west of Washington state. *J. Geodyn.,* 27(3):277–288. **doi:10.1016/S0264-3707(98)00001-5**

Ford, K.H., Naehr, T.H., Skilbeck, C.G., and the Leg 201 Scientific Party, 2003. The use of infrared thermal imaging to identify gas hydrate in sediment cores. *In* D'Hondt, S.L., Jørgensen, B.B., Miller, D.J., et al., *Proc. ODP, Init. Repts.,* 201: College Station, TX (Ocean Drilling Program), 1–20. **doi:10.2973/odp.proc.ir.201.104.2003**

Gerdom, M., Tréhu, A.M., Flueh, E.R., and Klaeschen, D., 2000. The continental margin off Oregon from seismic investigations. *Tectonophysics,* 329(1–4):79–97. **doi:10.1016/S0040-1951(00)00190-6**

Ginsburg, G., Soloviev, V., Matveeva, T., and Andreeva, I., 2000. Sediment grain-size control on gas hydrate presence, Sites 994, 995, and 997. *In* Paull, C.K., Matsumoto, R., Wallace, P.J., and Dillon, W.P. (Eds.), *Proc. ODP, Sci. Results,* 164: College Station, TX (Ocean Drilling Program), 237–245. **doi:10.2973/odp.proc.sr.164.236.2000**

Greinert, J., Bohrmann, G., and Suess, E., 2001. Gas hydrate-associated carbonates and methane-venting at Hydrate Ridge: classification, distribution and origin of authigenic lithologies. *In* Paul, C.K., and Dillon, W.P. (Eds.), *Natural Gas Hydrates: Occurrence, Distribution, and Detection*. Geophys. Monogr., 124:99–114.

Gulick, S.P.S., Meltzer, A.M., and Clarke, S.H., Jr., 1998. Seismic structure of the southern Cascadia subduction zone and accretionary prism north of the Mendocino triple junction. *J. Geophys. Res.,* 103(B11):27207–27222. **doi:10.1029/98JB02526**

Heeschen, K.U., Tréhu, A.M., Collier, R.W., Suess, E., and Rehder, G., 2003. Distribution and height of methane bubble plumes on the Cascadia margin characterized by acoustic imaging. *Geophys. Res. Lett.,* 30:1643–1646. **doi:10.1029/2003GL016974**

Hesse, R., and Harrison, W.E., 1981. Gas hydrates (clathrates) causing pore-water freshening and oxygen isotope fractionation in deep-water sedimentary sections of terrigenous continental margins. *Earth Planet. Sci. Lett.,* 55(3):453–462. **doi:10.1016/0012-821X(81)90172-2**

Holbrook, W.S., Hoskins, H., Wood, W.T., Stephen, R.A., Lizzarralde, D., and the Leg 164 Science Party, 1996. Methane gas-hydrate and free gas on the Blake Ridge from vertical seismic profiling. *Science,* 273:1840–1843.

Hovland, M., Lysne, D., and Whiticar, M., 1995. Gas hydrate and sediment gas composition, Hole 892A. *In* Carson, B., Westbrook, G.K., Musgrave, R.J., and Suess, E. (Eds.), *Proc. ODP, Sci. Results,* 146 (Pt. 1): College Station, TX (Ocean Drilling Program), 151–161.

Hyndman, R.D., Spence, G.D., Chapman, N.R., Riedel, M., and Edwards, R.N., 2001. Geophysical studies of marine gas hydrate in northern Cascadia. *In* Paull, C.K., and Dillon, W.P. (Eds.), *Natural Gas Hydrates, Occurrence, Distribution and Detection*. Geophys. Monogr., 124:273–295.

Hyndman, R.D., Wang, K., Yuan, T., and Spence, G.D., 1993. Tectonic sediment thickening, fluid expulsion, and the thermal regime of subduction zone accretionary prisms: the Cascadia margin off Vancouver Island. *J. Geophys. Res.,* 98:21865–21876.

Inagaki, F., Nunoura, T., Nakagawa, S., Teske, A., Lever, M., Lauer, A., Suzuki, M., Takai, K., Delwiche, M., Colwell, F.S., Nealson, K.H., Horikoshi, K., D'Hondt, S.L., and Jørgensen, B.B., 2006. Biogeographical distribution and diversity of microbes in methane hydrate-bearing deep marine sediments on the Pacific Ocean margin. *Proc. Natl. Acad. Sci. U. S. A.,* 103(8):2815–2820. **doi:10.1073/pnas.0511033103**

Janik, A., Goldberg, D., Collett, T., and Leg 204 Scientific Party, 2003. Azimuthal variability in gas hydrate concentration using LWD resistivity and density images. *Eos, Trans. Am. Geophys. Union,* 84(46)(Suppl.):OS51C-0875. (Abstract)

Johnson, J.E., Goldfinger, C., and Suess, E., 2003. Geophysical constraints on the surface distribution of authigenic carbonates across the Hydrate Ridge region, Cascadia margin. *Mar. Geol.,* 202(1-2):79–120. **doi:10.1016/S0025-3227(03)00268-8**

Kastner, M., Kvenvolden, K.A., Whiticar, M.J., Camerlenghi, A., and Lorenson, T.D., 1995. Relation between pore fluid chemistry and gas hydrates associated with bottom-simulating reflectors at the Cascadia margin, Sites 889 and 892. *In* Carson, B., Westbrook, G.K., Musgrave, R.J., and Suess, E. (Eds.), *Proc. ODP, Sci. Results,* 146 (Pt. 1): College Station, TX (Ocean Drilling Program), 175–187.

Kim, D.-Y., Uhm, T.-W., Lee, H., Lee, Y.-J., Ryu, B.-J., and Kim, J.-H., 2005. Compositional and structural identification of natural gas hydrates collected at Site 1249 on Ocean Drilling Program Leg 204. *Korean J. Chem. Eng.,* 22(4):1–4.

Knittel, K., Lösekann, T., Boetius, A., Kort, R., and Amann, R., 2005. Diversity and distribution of methanotrophic archaea at cold seeps. *Appl. Environ. Microbiol.,* 71(1):467–479. **doi:10.1128/AEM.71.1.467-479.2005**

Kraemer, L.M., Owen, R.M., and Dickens, G.R., 2000. Lithology of the upper gas hydrate zone, Blake Outer Ridge: a link between diatoms, porosity, and gas hydrate. *In* Paull, C.K., Matsumoto, R., Wallace, P.J., and Dillon, W.P. (Eds.), *Proc. ODP, Sci. Results,* 164: College Station, TX (Ocean Drilling Program), 229–236. **doi:10.2973/odp.proc.sr.164.221.2000**

Kulm, L.D., Suess, E., Moore, J.C., Carson, B., Lewis, B.T., Ritger, S.D., Kadko, D.C., Thornburg, T.M., Embley, R.W., Rugh, W.D., Massoth, G.J., Langseth, M.G., Cochrane, G.R., and Scamman, R.L., 1986. Oregon subduction zone: venting, fauna, and carbonates. *Science,* 231:561–566.

Kulm, L.D., von Huene, R., et al., 1973. *Init. Repts. DSDP,* 18: Washington (U.S. Govt. Printing Office).

Kumar, D.M., Sen, K., and Bangs, N.L., in press. Gas hydrate concentration from multicomponent seismic reflection data from Hydrate Ridge. *Geophysics.*

Kumar, D., Sen, M.K., Bangs, N.L., Wang, C., and Pecher, I., 2006. Seismic anisotropy at Hydrate Ridge. *Geophys. Res. Lett.,* 33(1):L01306. **doi:10.1029/2005GL023945**

Kvenvolden, K.A., 1995. A review of the geochemistry of methane in natural gas hydrate. *Org. Geochem.,* 23(11–12):997–1008. **doi:10.1016/0146-6380(96)00002-2**

Liu, X., and Flemings, P.B., 2006. Passing gas through the hydrate stability zone at southern Hydrate Ridge, offshore Oregon. *Earth Planet. Sci. Lett.,* 241(1–2):211–226. **doi:10.1016/j.epsl.2005.10.026**

MacKay, M.E., 1995. Structural variation and landward vergence at the toe of the Oregon accretionary prism. *Tectonics,* 14(6):1309–1320. **doi:10.1029/95TC02320**

MacKay, M.E., Jarrard, R.D., Westbrook, G.K., and Hyndman, R.D., 1994. Origin of bottom-simulating reflectors: geophysical evidence from the Cascadia accretionary prism. *Geology,* 22(5):459–462. **doi:10.1130/0091-7613(1994)022<0459:OOBSRG>2.3.CO;2**

MacKay, M.E., Moore, G.F., Cochrane, G.R., Moore, J.C., and Kulm, L.D., 1992. Landward vergence and oblique structural trends in the Oregon margin accretionary prism: implications and effect on fluid flow. *Earth Planet. Sci. Lett.,* 109(3-4):477–491. **doi:10.1016/0012-821X(92)90108-8**

Marchesi, J.R., Weightman, A.J., Cragg, B.A., Parkes, R.J., and Fry, J.C., 2001. Methanogen and bacterial diversity and distribution in deep gas hydrate sediments from the Cascadia margin as revealed by 16S rRNA molecular analysis. *FEMS Microbiol. Ecol.,* 34(3):221–228. **doi:10.1111/j.1574-6941.2001.tb00773.x**

Martin, J.B., Gieskes, J.M., Torres, M.E., and Kastner, M., 1993. Bromine and iodine in Peru margin sediments and pore fluids: implications for fluid origins. *Geochim. Cosmochim. Acta,* 57:4377–4389.

Milkov, A.V., Claypool, G.E., Lee, Y.-J., and Sassen, R., 2005. Gas hydrate systems at Hydrate Ridge offshore Oregon inferred from molecular and isotopic properties of gas hydrate-bound and void gases. *Geochim. Cosmochim. Acta,* 69(4):1007–1026. **doi:10.1016/j.gca.2004.08.021**

Milkov, A.V., Claypool, G.E., Lee, Y.-J., Torres, M.E., Borowski, W.S., Tomaru, H., Sassen, R., Long, P.E., and ODP Leg 204 Scientific Party, 2004a. Ethane enrichment and propane depletion in subsurface gases indicate gas hydrate occurrence in marine sediments at southern Hydrate Ridge offshore Oregon. *Org. Geochem.,* 35(9):1067–1080. **doi:10.1016/j.orggeochem.2004.04.003**

Milkov, A.V., Claypool, G.E., Lee, Y-J., Xu, W., Dickens, G.R., Borowski, W.S., and the ODP Leg 204 Scientific Party, 2003. In situ methane concentrations at Hydrate Ridge offshore Oregon: new constraints on the global gas hydrate inventory from an active margin. *Geology,* 31:833–836.

Milkov, A.V., Dickens, G.R., Claypool, G.E., Lee, Y-J., Borowski, W.S., Torres, M.E., Xu, W., Tomaru, H., Tréhu, A.M., and Schultheiss, P., 2004b. Co-existence of gas hydrate, free gas, and brine within the regional gas hydrate stability zone at Hydrate Ridge (Oregon Margin): evidence from prolonged degassing of a pressurized core. *Earth Planet. Sci. Lett.,* 222(3-4):829–843. **doi:10.1016/j.epsl.2004.03.028**

Milkov, A.V., and Xu, W., 2005. Comment on "Gas hydrate growth, methane transport, and chloride enrichment at the southern summit of Hydrate Ridge, Cascadia margin off Oregon" by Torres et al. [Earth Planet. Sci. Lett. 226 (2004) 225–241]. *Earth Planet. Sci. Lett.,* 239(1–2):162–167. **doi:10.1016/j.epsl.2005.05.044**

Musgrave, R.J., Bangs, N.L., Larrasoaña, J.C., Gràcia, E., Hollamby, J.A., and Vega, M.E., 2006. Rise of the base of the gas hydrate zone since the last glacial recorded by rock magnetism. *Geology,* 34:117–120. **doi:10.1130/G22008.1**

Oleskevich, D.A., Hyndman, R.D., and Wang, K., 1999. The updip and downdip limits to great subduction earthquakes: thermal and structural models of Cascadia, south Alaska, SW Japan and Chile. *J. Geophys. Res.,* 104(B7):14965–14992. **doi:10.1029/1999JB900060**

Orcutt, B., 2006. Diversity and function of Archaea in methane-rich marine habitats [Gordon Conference on Organic Geochemistry, 6–11 August 2006, Plymouth, NH].

Parkes, R.J., Webster, G., Cragg, B.A., Weightman, A.J., Newberry, C.J., Ferdelman, T.G., Kallmeyer, J., Jørgensen, B.B., Aiello, I.W., and Fry, J.C., 2005. Deep sub-seafloor prokaryotes stimulated at interfaces over geological time. *Nature (London, U. K.),* 436(7049):390–394. **doi:10.1038/nature03796**

Paull, C.K., Matsumoto, R., Wallace, P.J., et al., 1996. *Proc. ODP, Init. Repts.,* 164: College Station, TX (Ocean Drilling Program).

Riedel, M., Collett, T.S., and Hyndman, R.D. 2005. Gas hydrate concentration estimates from chlorinity, electrical resistivity, and seismic velocity. *Geol. Surv. Can. Open-File Rep.,* 4934.

Riedel, M., Long, P.E., and Collett, T.S., 2006. Estimates of in situ gas hydrate concentration from resistivity monitoring of gas hydrate bearing sediments during temperature equilibration. *Mar. Geol.,* 227(3–4):215–225. **doi:10.1016/j.margeo.2005.10.007**

Shipboard Scientific Party, 1994. Site 892. *In* Westbrook, G.K., Carson, B., Musgrave, R.J., et al., *Proc. ODP, Init. Repts.,* 146 (Pt. 1): College Station, TX (Ocean Drilling Program), 301–378.

Suess, E., Torres, M.E., Bohrmann, G., Collier, R.W., Greinert, J., Linke, P., Rehder, G., Tréhu, A., Wallmann, K., Winckler, G., and Zuleger, E., 1999. Gas hydrate destabili-

zation: enhanced dewatering, benthic material turnover and large methane plumes at the Cascadia convergent margin. *Earth Planet. Sci. Lett.,*170(1–2):1–15. **doi:10.1016/S0012-821X(99)00092-8**

Suess, E., Torres, M.E., Bohrmann, G., Collier, R.W., Rickert, D., Goldfinger, C., Linke, P., Heuser, A., Sahling, H., Heeschen, K., Jung, C., Nakamura, K., Greinert, J., Pfannkuche, O., Trehu, A., Klinkhammer, G., Whiticar, M.J., Eisenhauer, A., Teichert, B., and Elvert, M., 2001. Sea floor methane hydrates at Hydrate Ridge, Cascadia margin. *In* Paull, C.K., and Dillon, W.P. (Eds.), *Natural Gas Hydrates: Occurrence, Distribution, and Detection*. Geophys. Monogr., 124:87–98.

Teichert, B.M.A., Bohrmann, G., and Suess, E., 2005a. Chemoherms on Hydrate Ridge—unique microbially-mediated carbonate build-ups growing into the water column. *Palaeogeogr., Palaeoclimatol., Palaeoecol.,* 227(1–3):67–85. **doi:10.1016/j.palaeo.2005.04.029**

Teichert, B.M.A., Torres, M.E., Bohrmann, G., and Eisenhauer, A., 2005b. Fluid sources, fluid pathways and diagenetic reactions across an accretionary prism revealed by Sr and B geochemistry. *Earth Planet. Sci. Lett.,* 239(1–2):106–121. **doi:10.1016/j.epsl.2005.08.002**

Tomaru, H., Torres, M.E., Matsumoto, R., and Borowski, W., in press. Effect of massive gas hydrate formation on the water isotopic fractionation of the gas hydrate system at Hydrate Ridge, Cascadia margin offshore Oregon. *Geochem., Geophys., Geosyst.*

Torres, M.E., McManus, J., Hammond, D.E., de Angelis, M.A., Heeschen, K.U., Colbert, S.L., Tryon, M.D., Brown, K.M., and Suess, E., 2002. Fluid and chemical fluxes in and out of sediments hosting methane hydrate deposits on Hydrate Ridge, OR, I: Hydrological provinces. *Earth Planet. Sci. Lett.,* 201(3-4):525–540. **doi:10.1016/S0012-821X(02)00733-1**

Torres, M.E., Mix, A.C., Kinports, K., Haley, B., Klinkhammer, G.P., McManus, J., and de Angelis, M.A., 2003. Is methane venting at the seafloor recorded by $\delta^{13}C$ of benthic foraminifera shells? *Paleoceanography,* 18(3):1062–1075. **doi:10.1029/2002PA000824**

Torres, M.E., Teichert, B.M.A., Tréhu, A.M., Borowski, W., and Tomaru, H., 2004a. Relationship of pore water freshening to accretionary processes in the Cascadia margin: fluid sources and gas hydrate abundance. *Geophys. Res. Lett.,* 31:L22305. **doi:10.1029/2004GL021219**

Torres, M.E., Wallmann, K., Tréhu, A.M., Bohrmann, G., Borowski, W.S., and Tomaru, H., 2004b. Gas hydrate growth, methane transport, and chloride enrichment at the southern summit of Hydrate Ridge, Cascadia margin off Oregon. *Earth Planet. Sci. Lett.,* 226(1-2):225–241. **doi:10.1016/j.epsl.2004.07.029**

Torres, M.E., Wallmann, K., Tréhu, A.M., Bohrmann, G., Borowski, W.S., and Tomaru, H., 2005. Reply to comment on "Gas hydrate growth, methane transport and chloride enrichment at the southern summit of Hydrate Ridge, Cascadia margin off Oregon." *Earth Planet. Sci. Lett.,* 239(1–2):168–175. **doi:10.1016/j.epsl.2005.08.012**

Tréhu, A.M., Bohrmann, G., Rack, F.R., Torres, M.E., et al., 2003. *Proc. ODP, Init. Repts.,* 204: College Station, TX (Ocean Drilling Program). **doi:10.2973/odp.proc.ir.204.2003**

Tréhu, A.M., Flemings, P.B., Bangs, N.L., Chevallier, J., Gràcia, E., Johnson, J.E., Liu, C.-S., Liu, X., Riedel, M., and Torres, M.E., 2004a. Feeding methane vents and gas hydrate deposits at south Hydrate Ridge. *Geophys. Res. Lett.,* 31:L23310. **doi:10.1029/2004GL021286**

Tréhu, A.M., and Flueh, E.R., 2001. Estimating the thickness of the free gas zone beneath Hydrate Ridge, Oregon continental margin, from seismic velocities and attenuation. *J. Geophys. Res.,* 106(B2):2035–2046. **doi:10.1029/2000JB900390**

Tréhu, A.M., Long, P.E., Torres, M.E., Bohrmann, G., Rack, F.R., Collett, T.S., Goldberg, D.S., Milkov, A.V., Riedel, M., Schultheiss, P., Bangs, N.L., Barr, S.R., Borowski, W.S., Claypool, G.E., Delwiche, M.E., Dickens, G.R., Gracia, E., Guerin, G., Holland, M., Johnson, J.E., Lee, Y.-J., Liu, C.-S., Su, X., Teichert, B., Tomaru, H., Vanneste, M.,

Watanabe, M., and Weinberger, J.L., 2004b. Three-dimensional distribution of gas hydrate beneath southern Hydrate Ridge: constraints from ODP Leg 204. *Earth Planet. Sci. Lett.,* 222(3–4):845–862. **doi:10.1016/j.epsl.2004.03.035**

Tréhu, A.M., Ruppel, C., Holland, M., Dickens, G.R., Torres, M.E., Collett, T.S., Goldberg, D., Riedel, M., and Schultheiss, P., in press. Gas hydrates in marine sediments: lessons from scientific drilling. *Oceanography.*

Tréhu, A.M., Torres, M.E., Moore, G.F., Suess, E., and Bohrmann, G., 1999. Temporal and spatial evolution of a gas hydrate-bearing accretionary ridge on the Oregon continental margin. *Geology,* 27(10):939–942. **doi:10.1130/0091-7613(1999)027<0939:TASEOA>2.3.CO;2**

Ussler, W., III, and Paull, C.K., 2001. Ion exclusion associated with marine gas hydrate deposits. *In* Paull, C.K., and Dillon, W.P. (Eds.), *Natural Gas Hydrates: Occurrence, Distribution, and Detection.* Geophys. Monogr., 124:41–51.

Wang, K., Hyndman, R.D., and Davis, E.E., 1993. Thermal effects of sediment thickening and fluid expulsion in accretionary prisms: model and parameter analysis. *J. Geophys. Res.,* 98:9975–9984.

Weinberger, J.L., and Brown, K.M., 2006. Fracture networks and hydrate distribution at Hydrate Ridge, Oregon. *Earth Planet. Sci. Lett.,* 245:123–136.

Weinberger, J.L., Brown, K.M., and Long, P.E., 2005. Painting a picture of gas hydrate distribution with thermal images. *Geophys. Res. Lett.,* 32(4):L04609. **doi:10.1029/2004GL021437**

Westbrook, G.K., Carson, B., Musgrave, R.J., et al., 1994. *Proc. ODP, Init. Repts.,* 146 (Pt. 1): College Station, TX (Ocean Drilling Program).

Xu, W., 2004. Modeling dynamic marine gas hydrate systems. *Am. Mineral.,* 89:1271–1279.

Figure F1. A. Regional bathymetric map showing the locations of sites drilled during DSDP Leg 18 (Sites 174–76), ODP Leg 146 (Sites 888–892), ODP Leg 204, and IODP Expedition 311. Individual sites are not shown for Leg 204; the red box shows the location of the map in Figure F2A, p. 27. Plate boundaries and the relative motion vector between the Juan de Fuca and North America plates are also shown.

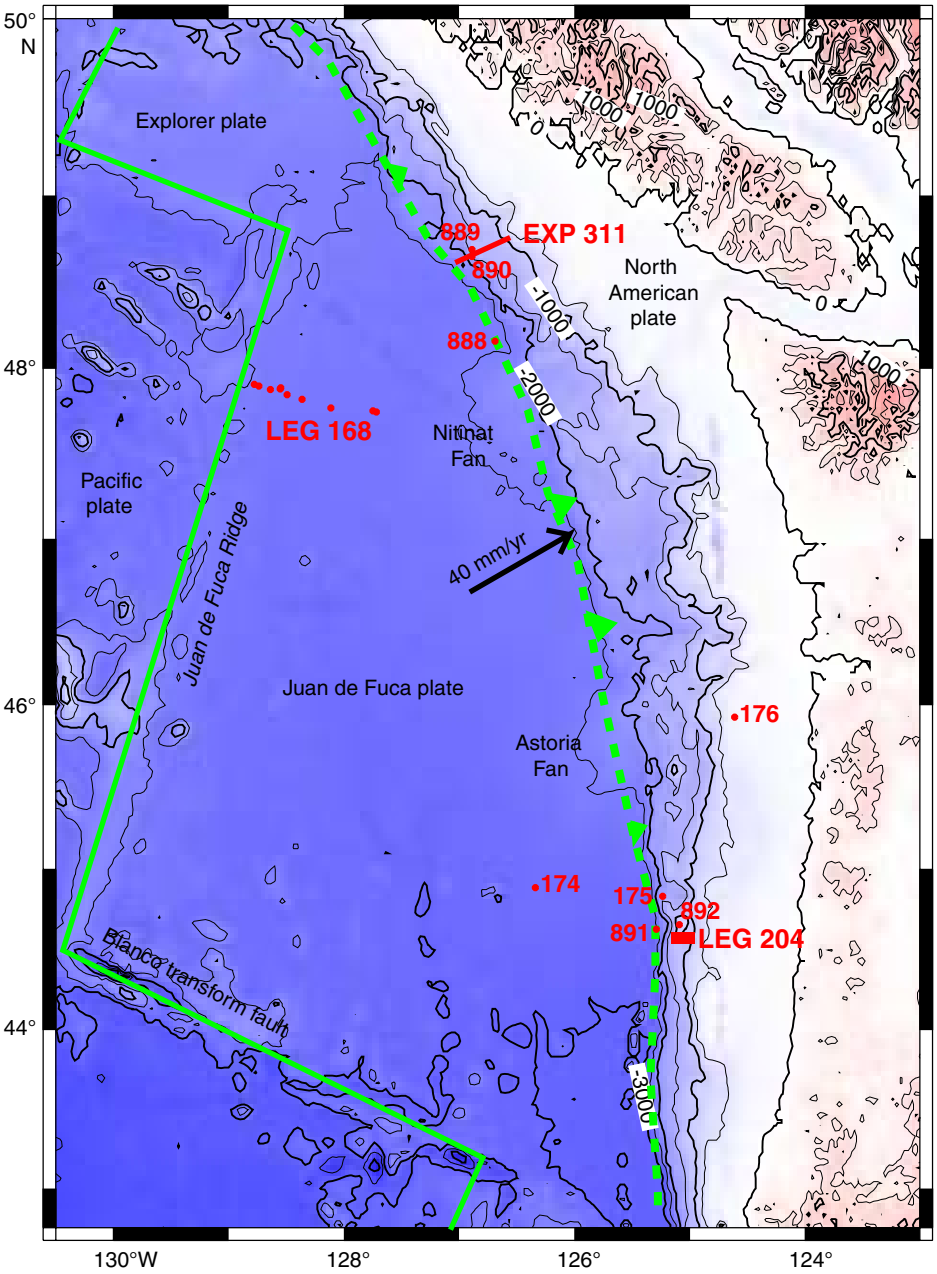

Figure F2. A. Map showing sites drilled during Leg 204. Locations of vertical slices from the 3-D seismic volume are also shown. Colored shading shows the gas hydrate content of the sediments averaged from the seafloor to the bottom-simulating reflector (BSR). Numbers in parentheses indicate the color scale for B–F. **B–F.** Slices from the 3-D seismic volume. Gas hydrate content in different regions is shown by color overlays. A, B, and B′ are bright reflections that were found to correspond to relatively coarse grained strata containing volcanic ash. AC is the older, more lithified and fractured, accreted sediments, which are overlain by uplifted and slightly deformed slope basin sediments (adapted from Tréhu et al., 2004b).

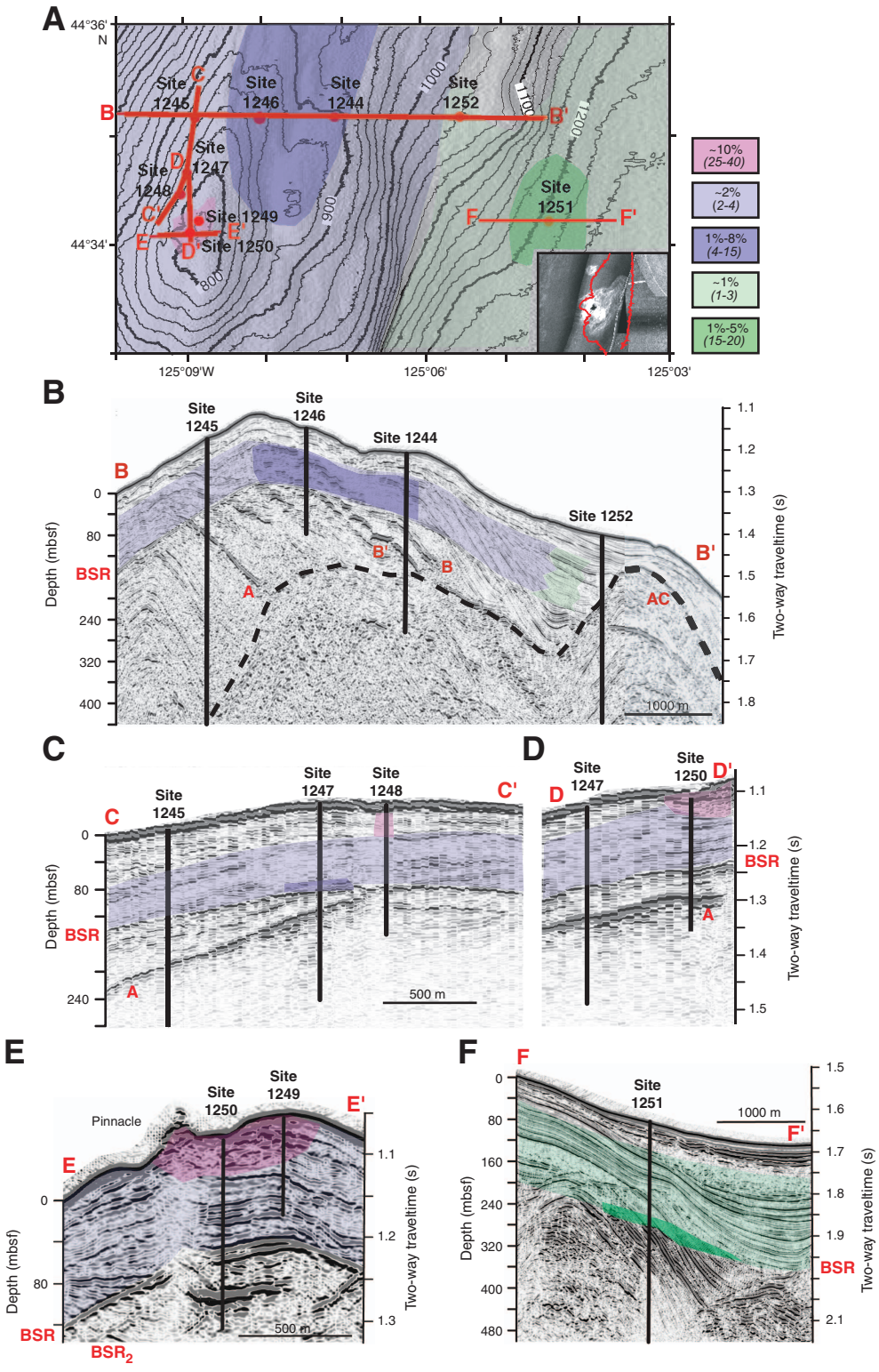

Figure F3. **A.** Seismic Profile OR89_Line2 through south Hydrate Ridge from the site survey conducted for Leg 146 (MacKay et al., 1992). Box shows the location of the section shown in C. The subduction zone décollement (DC), top of oceanic crust (TOC), accretionary complex (AC), and bottom-simulating reflector (BSR; dashed) are shown. **B.** Interpreted seismic section from A converted to depth using the velocity model of Gerdom et al. (2000), which was derived from large-aperture data recorded on ocean-bottom seismometers. Abyssal plain and accreted sediments are shown in shades of green; slope basin sediments are shown in light pink. **C.** Slice from the 3-D seismic survey coincident with the seismic section in A. Overlay shows seismic stratigraphic units discussed by **Chevallier et al.** (this volume). A, B, and B′ are bright reflections that were found to correspond to relatively coarse grained strata containing volcanic ash; AC indicates older, more lithified and fractured accreted sediments, which are overlain by uplifted and slightly deformed slope basin sediments; DBF1 and DBF2 are large debris flow deposits that indicate abrupt burial events, which may have affected gas hydrate stability; U is a regional unconformity that results from a migrating locus of uplift; F1 is a landward-vergent thrust fault from an earlier stage of accretion (adapted from **Chevallier et al.,** this volume). Although structural details of the accretionary history of AC are not well imaged, the total volume of sediment that has undergone accretion, subduction, duplexing, and underplating can be determined from these data.

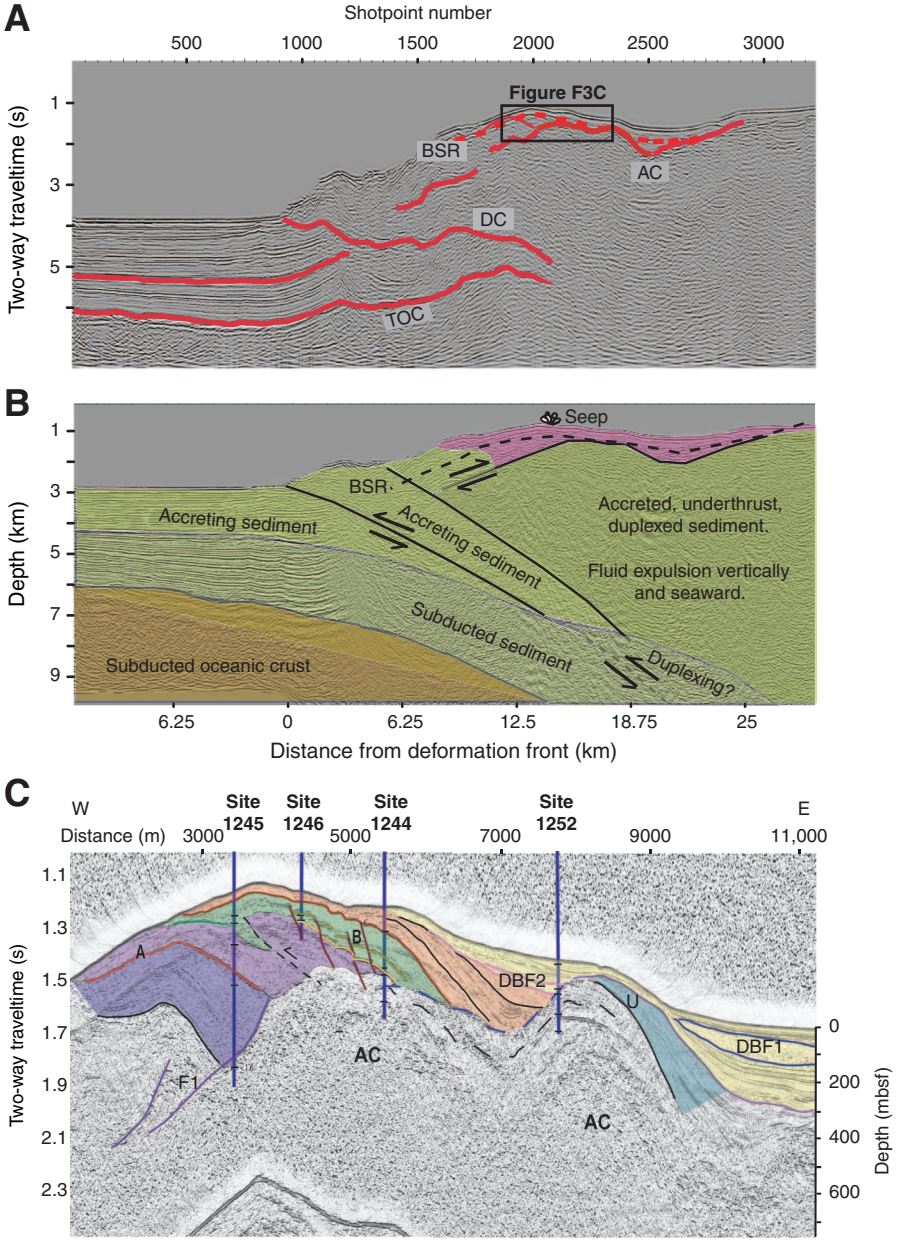

Figure F4. **A.** Modeled concentration vs. depth profile of methane estimated from projected and measured alkalinity concentrations as a function of depth at Site 1244. Red lines denote thermodynamic phase boundaries, showing that in situ methane production at this site reaches saturation levels with respect to gas hydrate at ~50 mbsf (shown by arrow). **B.** Methane production rates estimated from steady-state assumptions and exponential curve fit of alkalinity and methane concentration profiles. **C.** Gas composition and isotopic composition of methane at Site 1244, which indicate a biogenic methane source (see **Claypool et al.,** this volume). The high rates of methane production in the upper 50 mbsf correspond to the very light isotopic composition of the methane (highlighted by blue line).

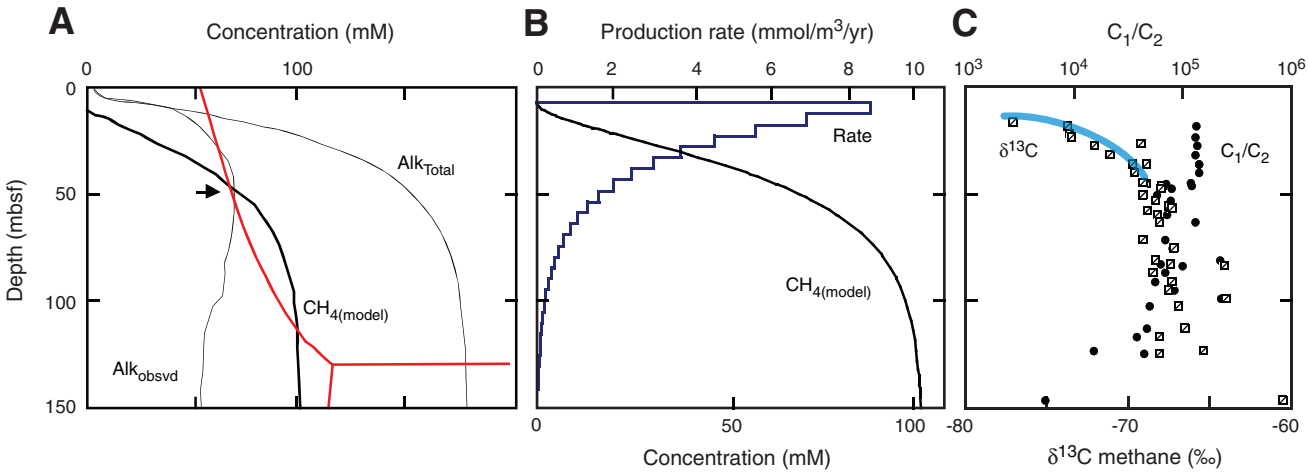

Figure F5. A. Amplitude of Horizon A. Gas saturation of 50%–90% of pore space is inferred from low in situ density values measured with LWD at Sites 1245, 1247, 1248, and 1250. White lines indicate the depth of Horizon A below sea level. The onset of large-amplitude anomalies along Horizon A is interpreted to indicate the base of a connected free gas column. Although Horizon A continues to the west of where it intersects the bottom-simulating reflector (BSR), its amplitude decreases abruptly and it cannot be unambiguously identified. **B.** Lithostatic stress (σ_L) compared to gas pressure (P_g) in Horizon A. Assuming that gas pressure is in equilibrium with hydrostatic pressure (P_w) at the base of the connected gas column, gas pressure in Horizon A exceeds the lithostatic stress at Site 1250. **C.** Effective gas stress on Horizon A. Topographic contours at a 20-m interval are also shown (black lines). Effective gas stress is negative beneath most of the summit. (A–C adapted from Tréhu et al., 2004a.) (Continued on next two pages.)

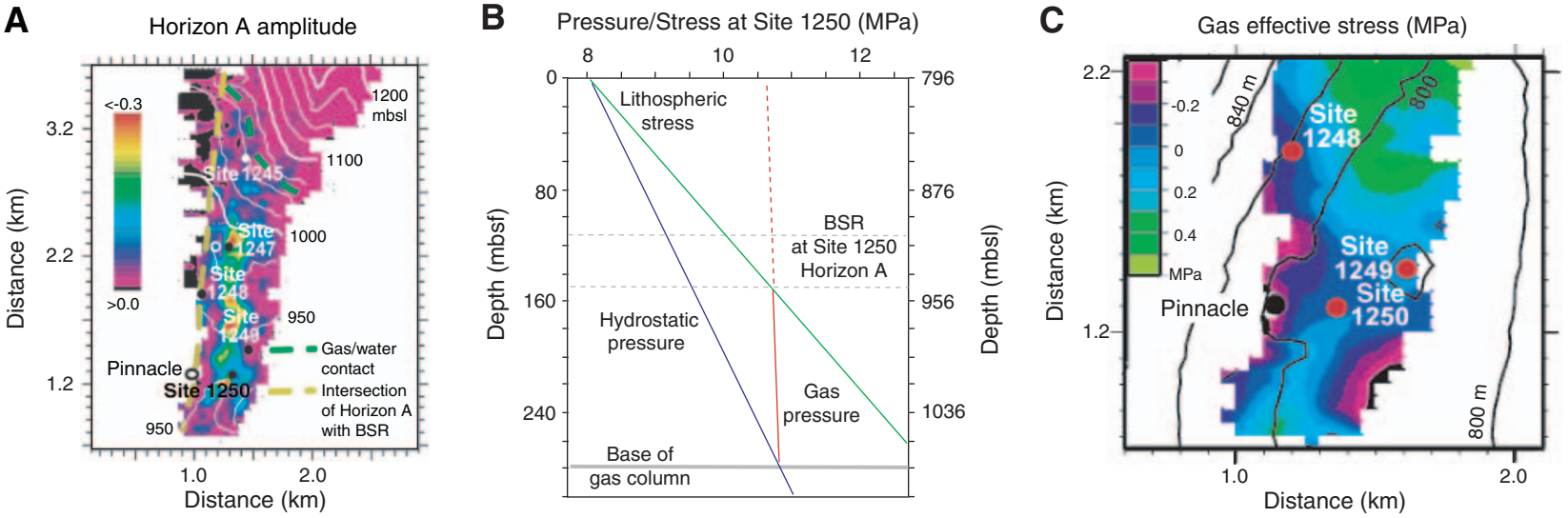

Figure F5 (continued). D. In situ bulk density (from LWD) and grain size distribution at Site 1245, which illustrate the anomalous nature of Horizon A. **E.** C_1/C_2 ratio and isotopic composition of methane at Sites 1245 and 1247, which shows anomalous geochemistry (low C_1/C_2; high $\delta^{13}C$) associated with Horizon A. Gas chemistry within the GHSZ is characteristic of biogenic gas. **F.** C_1/C_2 ratio and isotopic composition of methane at the summit. Gas chemistry indicates migrated gas both in Horizon A and in the upper 20–30 mbsf. The BSR is located at approximately the same depth at all three sites shown here. (D adapted from Tréhu et al., 2004a; E and F adapted from **Claypool et al.,** this volume.) (Continued on next page.)

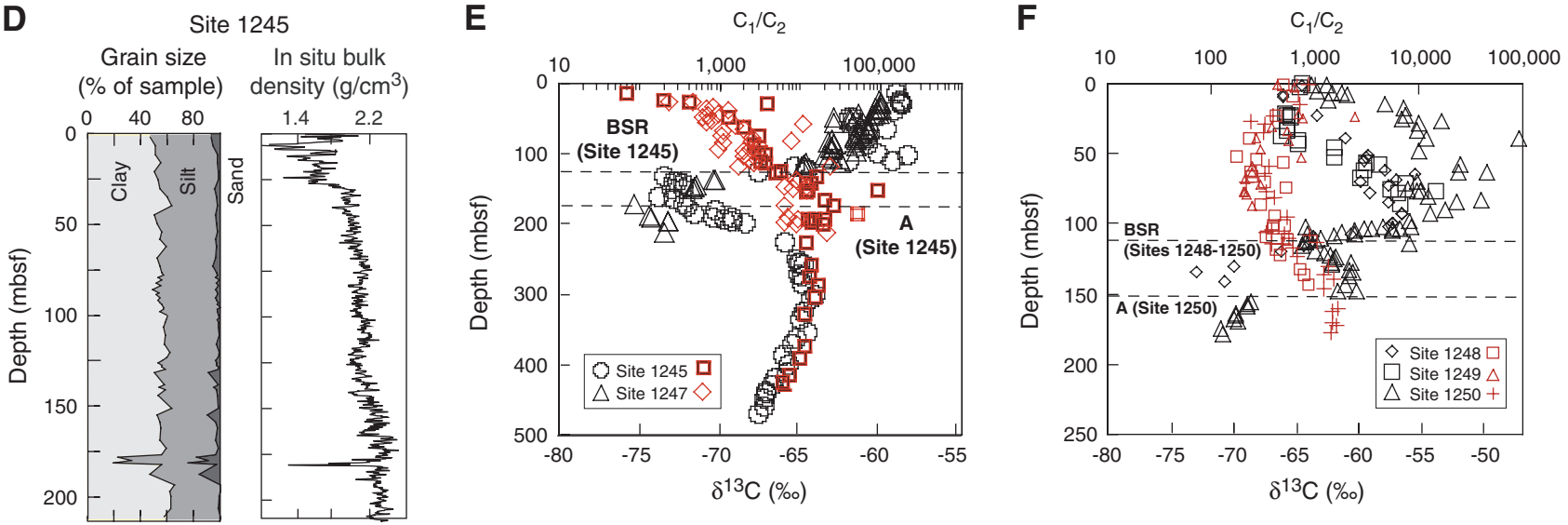

Figure F5 (continued). G. *P*- and *S*-wave velocities from sonic logs and a vertical seismic profile (VSP). Horizon A appears as a pronounced low-velocity zone in V_S and V_P (VSP only). The absence of a V_P anomaly in the sonic log data may result from intrusion of drilling fluid near the borehole. The V_S anomaly is unexpected, since V_S is not sensitive to whether the pore space is occupied by water or gas, and suggests that overpressures are large enough to affect the sediment shear strength. **H.** Increase in effective stress (σ_e) with depth, as calculated from sediment bulk density at Site 1249 compared to the internal pressures of gas hydrate crystallite (P_h) and gas bubbles (P_g) calculated following Clennell et al. (1999) assuming an average pore radius of 0.5 mm, compared to Cl^- enhancement and gas hydrate saturation predicted by a one-dimensional transport reaction model with enhanced gas dissolution and hydrate precipitation rates in near-surface sediments. Model parameters are described in Torres et al. (2004b). Cl^- concentrations measured at Site 1249 (squares) and IR anomalies at Sites 1249 (green bars) and 1250 (blue bars) are also shown. **I.** Seismic cross section at the summit showing the steady-state gas migration path suggested by Liu and Flemings (2006) and Milkov and Xu (2005) as a green line, compared to two possible paths (from among a wide range of possible paths) in the distributed, temporally variable scenario hypothesized by Tréhu et al. (2004b), Torres et al. (2004b), and Weinberger and Brown (2006). (G adapted from **Tréhu et al.,** this volume; H adapted from Torres et al., 2004b; I adapted from Tréhu et al., 2004a).

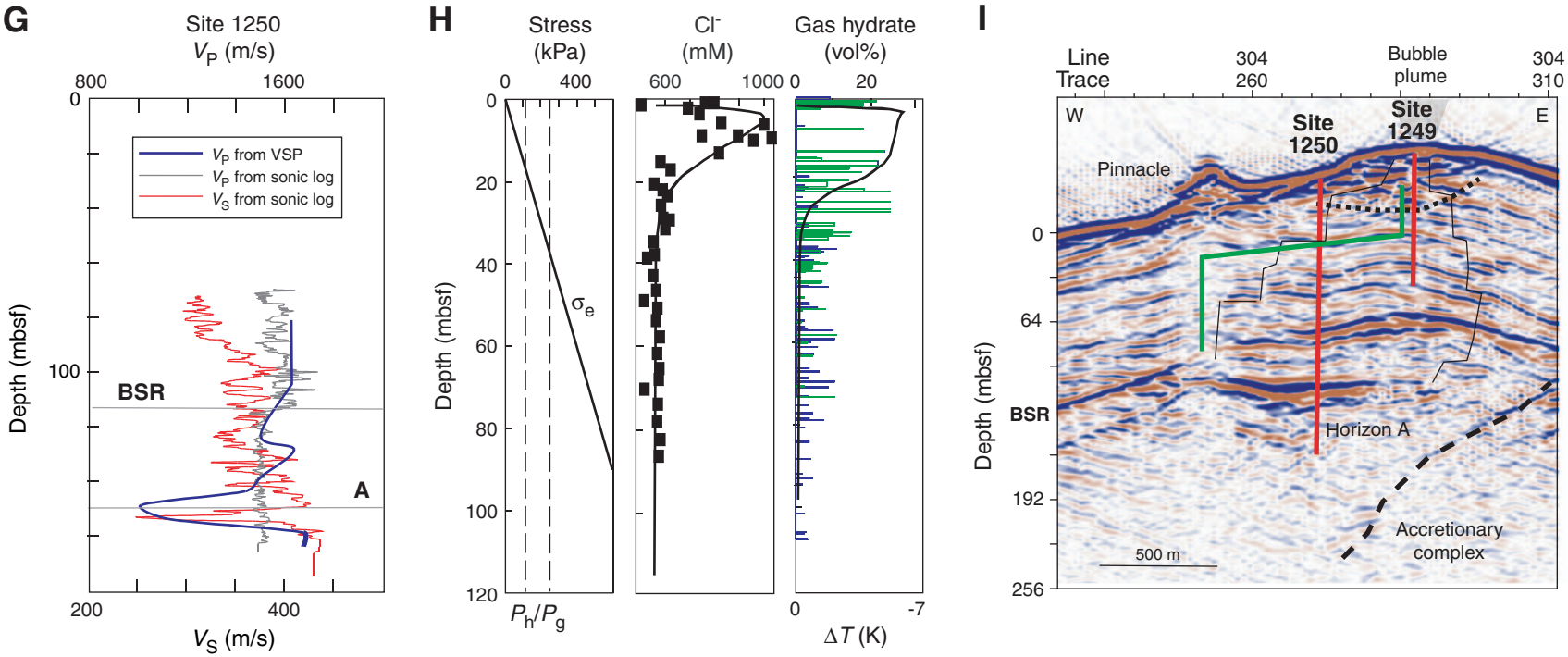

Figure F6. Nested view of data from Horizon B in Hole 1246B. **A.** Amount of gas hydrate estimated from pore water Cl^- anomalies in the entire hole (red dots), expressed as the percentage of pore space occupied by gas hydrate. **B.** Seismic image of Horizon B. **C.** IR temperature anomalies, magnetic susceptibility, and lithologic log for Core 204-1246B-8H showing the magnetic signature of a thick turbidite sequence. Large IR anomalies are associated with coarse-grained sediments (yellow) at the base of this turbidite. A similar turbidite sequence was observed in Core 204-1246B-7H. **D.** Detail of the 2-m-thick zone of IR anomalies. Black line is temperature recorded along the center line of the IR image of the core (yellow = 14°C, black = 8°C). The red line shows the simplified temperature profile used by Tréhu et al. (2004b) to estimate an average gas hydrate content of ~28% in the pore space in this interval from IR data. This estimate is similar to the estimate of 22% obtained from a pore water sample from this zone.

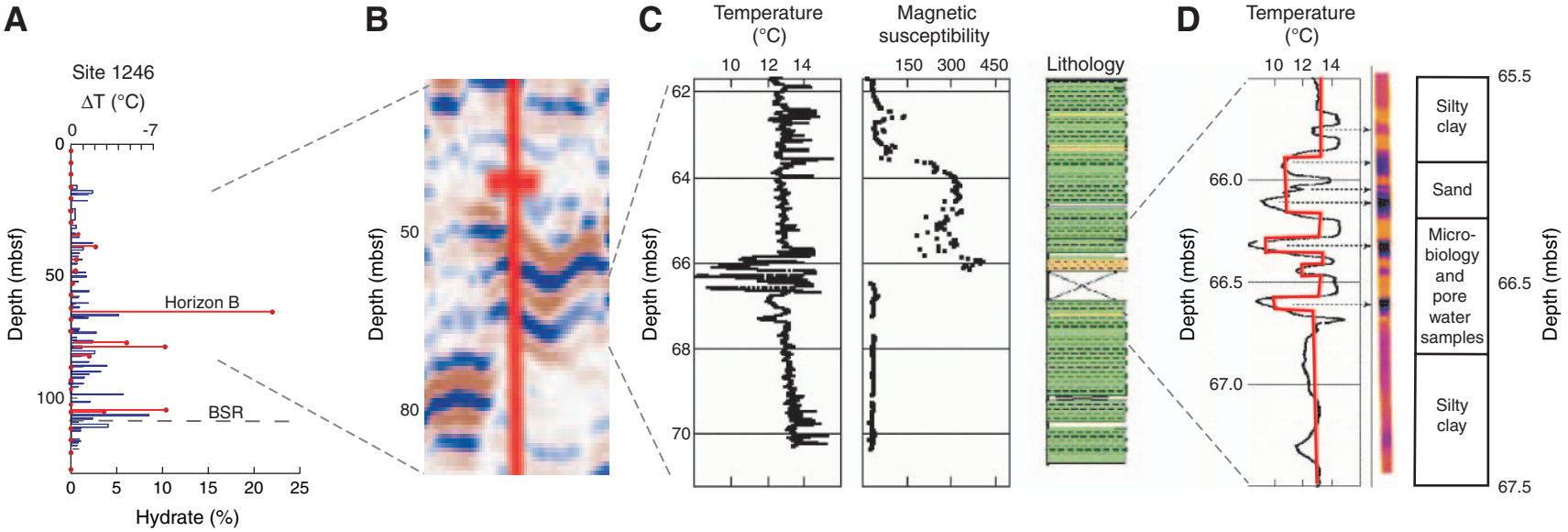

Figure F7. Data from Site 1251 illustrate lateral variability among holes a few tens of meters apart at the same site. **A.** Vertical slice through the seismic data. Note variable amplitude and character of the bottom-simulating reflector (BSR). Site 1251 sampled a spot within the slope basin east of Hydrate Ridge (Fig. F2, p. 27) where the BSR was unusually bright. **B.** Resistivity-at-the-bit (RAB) image from LWD data in Hole 1251A. Gas hydrate saturation calculated from the RAB data is also shown (note: because gas hydrate and free gas both increase the electrical resistivity, below the BSR, this should be interpreted as free gas saturation). In Hole 1251A, the presence of gas hydrate is indicated at 90–110 mbsf and free gas is indicated below the BSR, at 190–200 mbsf. The 10-m uncertainty in BSR depth is due to uncertainty in the seismic velocity used to convert the seismic data to depth. **C.** Gas hydrate concentration estimated from Cl^- (red line) and pressure core sampling (PCS) (green stars) data (Tréhu et al., 2004b) compared to IR temperature anomalies (blue bars). Three out of five PCS cores indicate methane supersaturation, although no Cl^- anomalies and very few IR anomalies were observed shallower than 190 mbsf. The inset shows a zone of very large IR and Cl^- anomalies at 188–200 mbsf. In Hole 1251B, the only other deep cored hole at this site, this depth interval was not recovered. Initial interpretation of the RAB data in B was that the BSR was at 190 mbsf and that there was free gas below the BSR but no significant gas hydrate deposit above the BSR in this hole. The difference in BSR depth between Hole 1251A and 1251D, located ~40 m away, was attributed to uncertainty in BSR depth (note short wavelength variations in BSR depth in the seismic data) and uncertainties in the drilling depths. An alternative interpretation is that the BSR is at 200 mbsf at 1251A and 1251D and that the upper 12 m of the deep resistivity anomaly at 1251A is due to gas hydrate.

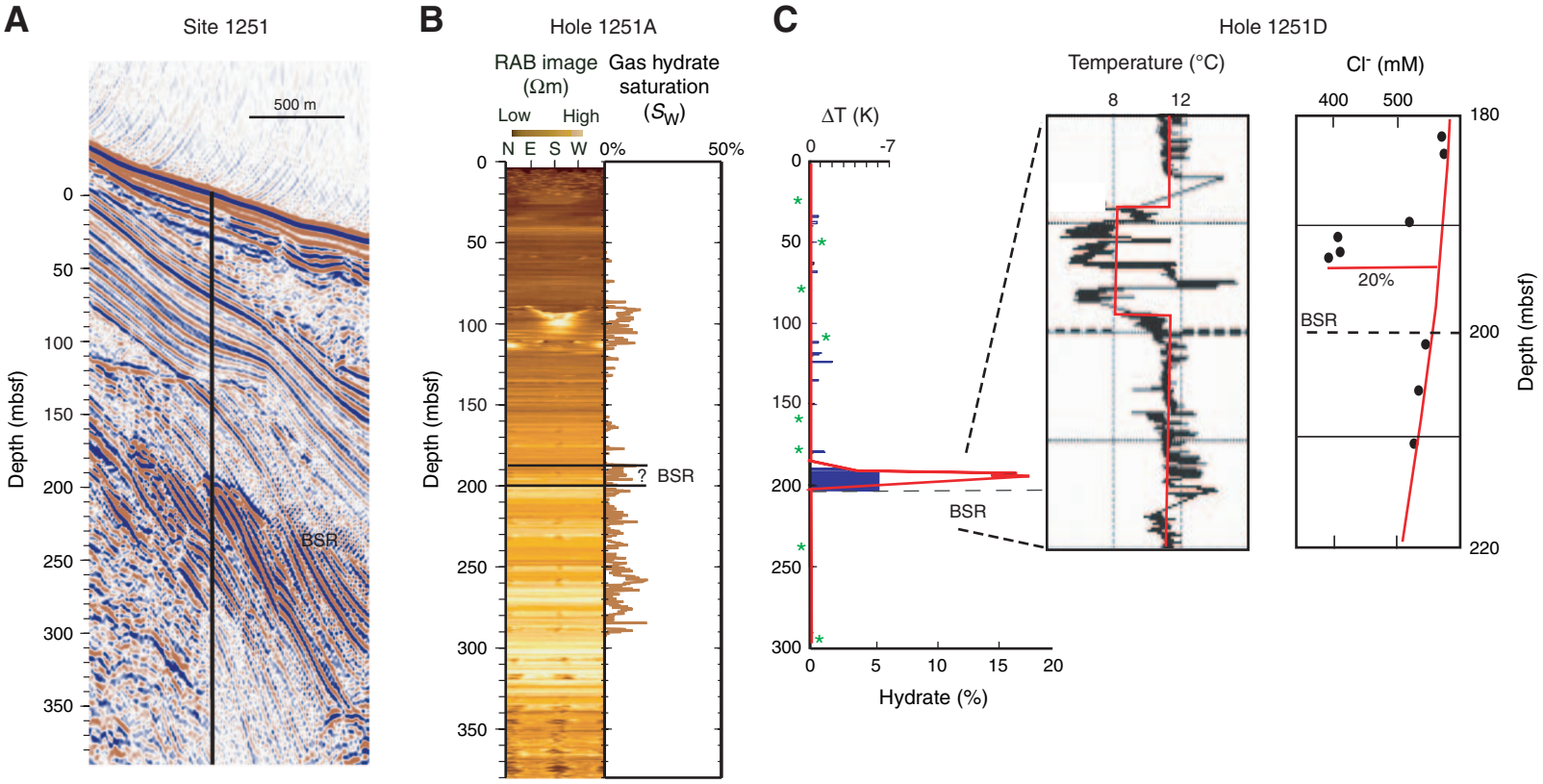

Figure F8. A. Gamma density profiles of a HYACINTH pressure core for ODP Leg 204 as pressure was released (Tréhu, Bohrmann, Rack, Torres, et al., 2003). At in situ conditions, a gas hydrate–rich zone at ~37 cm appears as a small low-density anomaly (run 1). Density decreases dramatically as pressure is released and the gas hydrate decomposes (run 12). After the core has been degassed, the bulk density of the sediment without hydrate is measured (run 16). **B.** IR image of several meters of core on either side of the HYACINTH pressure core. Dark horizontal lines represent cold anomalies (8°C) resulting from gas hydrate decomposition; yellow lines represent warm anomalies (14°C) resulting from voids due to gas expansion; background core temperature (pink) is ~12°C. There are no indications of gas hydrate in the upper 30 m, and gas hydrate is found in clusters of thin lenses spaced 2–3 m apart on average between 30 mbsf and the bottom-simulating reflector (BSR). The approximate length and spacing of pore water samples is also shown to illustrate the spatial relationship between the distribution of gas hydrate lenses to the spacing of pressure core and pore water samples (Tréhu et al., 2004b). **C.** Cl^- concentration measured in Hole 1244C (black dots). In contrast to Figures **F6,** p. 33, and **F7,** p. 34, the concentrations in this figure have not been converted to gas hydrate amount as a percentage of pore space to illustrate the sensitivity of these estimates to assumptions about the background Cl^- concentration (Ussler and Paull, 2001). If the pore water Cl^- concentration is assumed to be the same as seawater, a gradually increasing amount of gas hydrate with depth, superimposed on discrete lenses of higher concentration, is determined. Torres et al. (2004a) argue that the Cl^- concentration at SHR decreases with depth because of the input of freshwater from clay dehydration at depth and that the appropriate baseline should be defined as the envelope of the data (black line, referred to as the empirical baseline model). Assuming an empirical baseline, only discrete lenses with gas hydrate content up of up to 9% of the pore space (averaged over a 5- to 10-cm-long sample) are present at this site. The empirical baseline model is generally compatible with other gas hydrate proxy data from Leg 204 (Tréhu et al., 2004b). Methane concentration from pressure core data (red boxes) are overlain on the Cl^- data along with the gas hydrate phase diagram (red lines). Two pressure cores at this site likely contained gas hydate. **D.** Resistivity-at-the-bit (RAB) data from LWD operations in Hole 1244D. A detail from 66 to mbsf is shown as well as an image of the entire hole. Bright regions (high resistivity) are indicative of gas hydrate when they also correspond to low-density zones. The detail shows considerable azimuthal variation in gas hydrate distribution, suggesting that the gas hydrate forms in steeply dipping faults and fractures in this interval (Janik et al., 2003; Weinberger and Brown, 2006). It is interesting to note that the zone of dipping hydrate lenses suggested by the RAB data in Hole 1244D corresponds to a depth interval with only very small Cl^- anomalies in Hole 1244B, suggesting strong horizontal, as well as vertical, heterogeneity in hydrate distribution. (**Figure shown on next page.**)

Figure F8 (continued). (Caption shown on previous page.)

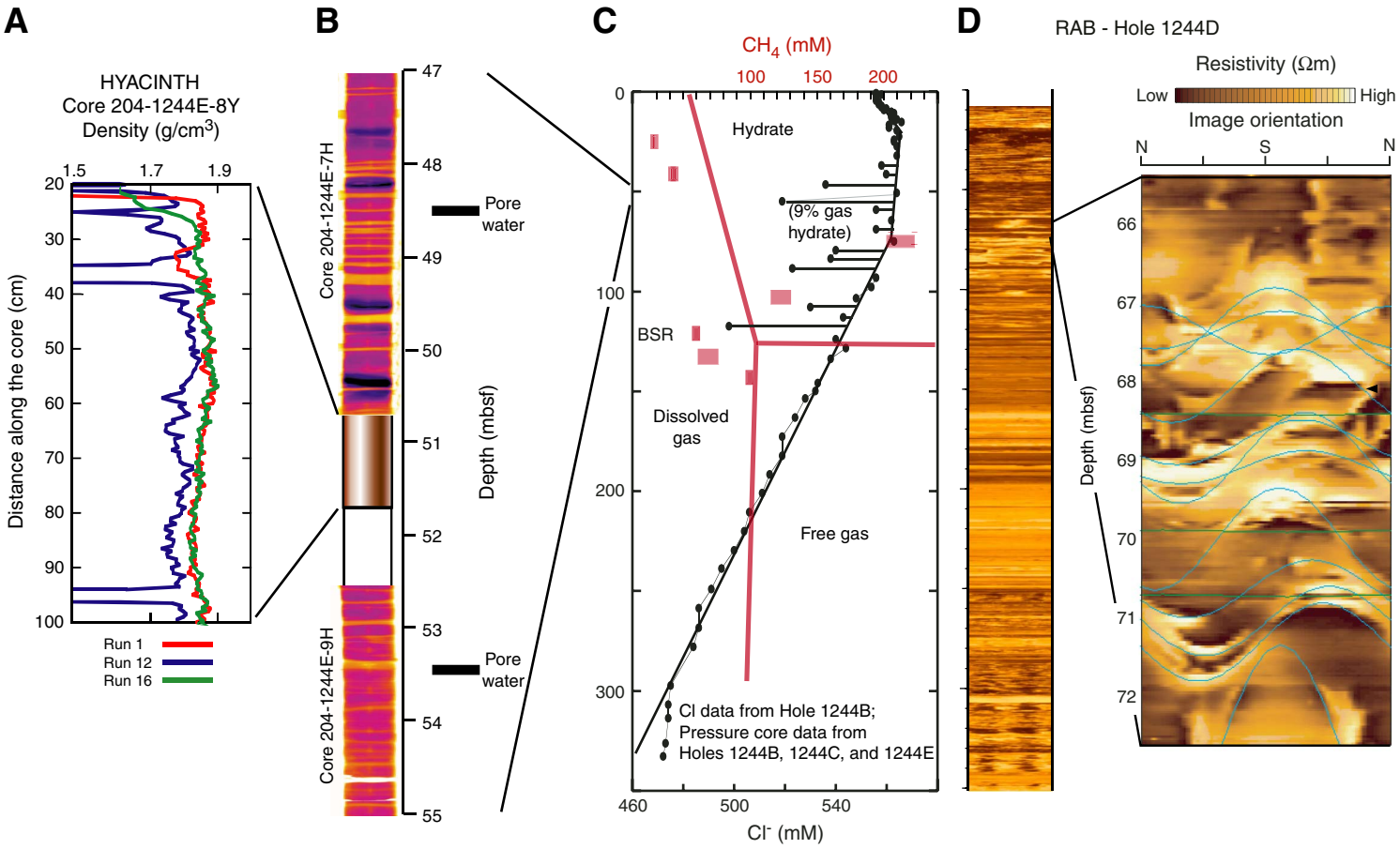

Table T1. Leg 204 site summary.

Hole	Latitude	Longitude	Seafloor (mbrf)	Number of cores	Cored (m)	Recovered (m)	Recovery (%)	Drilled (m)	Penetration (m)	Time on hole (hr)	Time on hole (days)
204-											
1244A	44°35.1701′N	125°7.1906′W	Missed	1	9.5	9.99	105.2	0.0	9.5	10.75	0.45
1244B	44°35.1702′N	125°7.1917′W	906.9	6	54.1	56.85	105.1	0.0	54.1	11.75	0.49
1244C	44°35.1784′N	125°7.1902′W	906.0	39	332.0	315.87	95.1	1.5	333.5	64.75	2.70
1244D	44°35.1865′N	125°7.1900′W	906.0	0	0.0	0.00	NA	380.0	380.0	37.50	1.56
1244E	44°35.1709′N	125°7.1719′W	904.8	19	135.8	137.73	101.4	114.2	250.0	74.75	3.11
1244F	44°35.1691′N	125°7.1705′W	907.4	4	24.1	24.90	103.3	0.0	0.0	5.00	0.21
			Site 1244 totals:	69	555.5	545.34	98.2	495.7	1027.1	204.50	8.52
1245A	44°35.1697′N	125°8.9462′W	886.5	0	0.0	0.00	NA	380.0	380.0	28.75	1.20
1245B	44°35.1587′N	125°8.9455′W	881.0	53	471.7	418.27	88.7	2.0	473.7	80.50	3.35
1245C	44°35.1702′N	125°8.9316′W	880.0	29	198.7	185.31	93.3	3.0	201.7	32.75	1.36
1245D	44°35.1690′N	125°8.9312′W	881.5	3	24.0	24.82	103.4	0.0	24.0	3.50	0.15
1245E	44°35.1702′N	125°8.9605′W	881.0	8	66.6	18.5	27.7	473.7	540.3	104.50	4.35
			Site 1245 totals:	93	761.0	646.88	85.0	858.7	1619.7	250.00	10.42
1246A	44°35.1642′N	125°8.1400′W	861.5	0	0.0	0.00	NA	180.0	180.0	18.25	0.76
1246B	44°35.1644′N	125°8.1235′W	860.8	16	136.7	135.34	99.0	0.0	136.7	18.75	0.78
			Site 1246 totals:	16	136.7	135.34	99.0	180.0	316.7	37.00	1.54
1247A	44°34.6591′N	125°9.0096′W	845.0	0	0.0	0.00	NA	270.0	270.0	21.25	0.89
1247B	44°34.6589′N	125°9.0766′W	845.9	27.0	217.0	212.0	97.7	3.0	220.0	60.5	2.52
			Site 1247 totals:	27	217.0	212.00	NA	273.0	490.0	81.75	3.41
1248A	44°34.4515′N	125°9.1548′W	843.0	0	0.0	0.00	NA	194.0	194.0	15.50	0.65
1248B	44°34.4568′N	125°9.1482′W	841.0	3	17.0	7.45	43.8	0.0	17.0	10.75	0.45
1248C	44°34.45′N	125°9.1499′W	841.0	17	149.0	101.56	68.2	0.0	149.0	22.75	0.95
			Site 1248 totals:	20	166.0	109.01	65.7	194.0	360.0	49.00	2.04
1249A	44°34.2246′N	125°8.8423′W	788.5	0	0.0	0.00	NA	90.0	90.0	9.75	0.41
1249B	44°34.2106′N	125°8.8412′W	788.5	8	45.0	14.01	31.1	29.9	74.9	28.00	1.17
1249C	44°34.2368′N	125°8.8410′W	788.5	14	88.5	58.84	66.5	1.5	90.0	22.25	0.93
1249D	44°34.2222′N	125°8.8366′W	788.5	3	16.5	4.78	29.0	2.0	18.5	5.25	0.22
1249E	44°34.2270′N	125°8.8369′W	788.5	3	9.0	4.38	48.7	2.0	11.0	4.75	0.20
1249F	44°34.2317′N	125°8.8377′W	788.5	16	82.5	57.37	69.5	7.5	90.0	22.75	0.95
1249G	44°34.2073′N	125°8.8416′W	788.5	5	43.0	11.24	26.1	0.0	43.0	9.00	0.38
1249H	44°34.2108′N	125°8.8365′W	788.5	6	52.5	27.52	52.4	0.0	52.5	8.50	0.35
1249I	44°34.2111′N	125°8.8437′W	788.5	4	33.6	8.69	25.9	0.0	33.6	6.00	0.25
1249J	44°34.2114′N	125°8.8422′W	788.5	3	32.5	7.69	23.7	0.0	32.5	5.50	0.23
1249K	44°34.2137′N	125°8.8392′W	788.5	5	43.2	16.87	39.1	1.0	44.2	8.25	0.34
1249L	44°34.2119′N	125°8.8439′W	788.5	5	38.5	14.15	36.8	0.0	38.5	10.25	0.43
			Site 1249 totals:	72	484.8	225.54	46.5	133.9	618.7	140.25	5.84
1250A	44°34.1176′N	125°9.0179′W	807.0	0	0.0	0.00	NA	210.0	210.0	20.25	0.84
1250B	44°34.1174′N	125°8.9921′W	807.0	0	0.0	0.00	NA	180.0	180.0	19.50	0.81
1250C	44°34.1273′N	125°9.0178′W	807.0	19	143.0	117.29	82.0	2.0	145.0	28.50	1.19
1250D	44°34.1063′N	125°9.0182′W	807.0	19	142.0	133.56	94.1	3.0	145.0	26.00	1.08
1250E	44°34.1124′N	125°9.0171′W	807.0	2	16.0	11.93	74.6	0.0	16.0	3.50	0.15
1250F	44°34.1166′N	125°9.0025′W	807.0	13	77.0	70.10	91.0	103.0	180.0	74.25	3.09
			Site 1250 totals:	53	378.0	332.88	88.1	498.0	876.0	172.00	7.17
1251A	44°34.2197′N	125°4.4521′W	1228.0	0	0.0	0.00	NA	380.0	380.0	25.25	1.05
1251B	44°34.2191′N	125°4.4375′W	1224.4	53	442.1	368.56	83.4	3.0	445.1	86.25	3.59
1251C	44°34.2058′N	125°4.4366′W	1221.4	2	17.6	13.63	77.4	0.0	17.6	4.50	0.19
1251D	44°34.2060′N	125°4.4365′W	1221.4	30	226.5	194.40	85.8	4.0	230.5	38.25	1.59
1251E	44°34.2126′N	125°4.4358′W	1220.0	1	9.5	9.89	104.1	0.0	9.5	1.75	0.07
1251F	44°34.2159′N	125°4.4369′W	1220.0	1	9.5	9.92	104.4	0.0	9.5	0.25	0.01
1251G	44°34.2145′N	125°4.4364′W	1220.0	2	10.5	11.11	105.8	10.5	21.0	4.25	0.18
1251H	44°34.2089′N	125°4.4514′W	1220.0	0	0.0	0.00	NA	445.0	445.0	63.8	2.66
			Site 1251 totals:	89	715.7	607.51	84.9	842.5	1558.2	224.25	9.34
1252A	44°35.1671′N	125°5.5691′W	1051.0	28	259.8	253.79	97.7	0.0	259.8	51.00	2.13
			Site 1252 totals:	28	259.8	253.79	97.7	0.0	259.8	51.00	2.13
			Totals:	467	3674.5	3068.29	83.5	3475.8	7126.2	1209.75	50.41

Note: NA = not applicable. Table from Leg 204 *Initial Reports* volume (Tréhu, Bohrmann, Rack, Torres, et al., 2003).

Table T2. Average hydrate content of sediments expressed as percent of pore space estimated using several different proxies.

Hole	BSR depth (m)	Depth range of RAB or IR (m)	Estimated hydrate from proxy in GHOZ/GHSZ (%)			
			IR*	PCS*	Cl^-*	RAB
Hydrate Ridge—away from summit						
204-						
1244B	124					8.1/6.1
1244C	124	45–125	3.2/2.0	0/0	2.2/2	
1244E	124	23–121	2.6/2.1	0.9/1.4	3.5/1.8	
1245A	134					3.1/1.9
1245B	134	52–119	3.8/1.9		3.0/2.0	
1245C	134	44–120	2.9/1.6	4.0/6.0		
1246A	114					1.5/1.0
1246B	114	16–117	5.6/5.0		2.3/1.7	
1247A	124					2.0/1.6
1247B	130	16–116	1.9/1.5	1.3/2.6	1.5/0.8	
Hydrate Ridge—summit						
204-						
1248A	115					17/7
1248C	115	1–124	7.3		4.5	
	115	1–30	18		NB	
1249A	115					73/75
1249F	115	1–88†	13.9	23	NB	
	115	1–30	23.6	43	NB	
	115	30–88	11.8	4.6	2	
1250A	114					26/5
1250C	114	14–109	2.6	0.7	4.3	
	114	1–14			NB	
1250D	114	7–114	1.8	1.4		
Slope basin						
204-						
1251A	200					1.2/1.0
1251B	200	41–188	1.6/1.2	0.5/0.5	BD	
1251D	200	34–205	5.2/4.5	0.2/0.2	2.8/1.7	
1252A	170	19–183	1.9/1.3		BD	

Notes: Table adapted from Tréhu et al. (2004a). * = corrected for percent recovery. Average gas hydrate content from infrared (IR) data was calculated as discussed in Tréhu et al. (2004a). Results are shown for integration over the gas hydrate occurrence zone (GHOZ), defined as the depth range over which indicators for gas hydrate were observed, and for the gas hydrate stability zone (GHSZ), defined as the region from the seafloor to the bottom-simulating reflector (BSR). At Site 1252, the projected depth of the BSR was used. For the summit region, the GHOZ and the GHSZ are the same because indicators of gas hydrate presence extend from the BSR to the seafloor. At these sites, the gas hydrate content of the shallow zone of massive hydrate is given separately. Each pressure core sampler (PCS)-derived result represents the average of 1–3 samples spaced at unequal intervals, each averaging gas hydrate content over ~1 m. No PCS data were acquired in Holes 1245B, 1246B, 1248C, or 1252A. Measurement uncertainties are discussed elsewhere. Chloride-derived estimates represent averages of 1–30 samples/hole spaced at unequal intervals, each averaging gas hydrate content over 5–10 cm of core length. Uncertainties due to uncertainties in the baseline are estimated to be ±0.5%. BD = any hydrate present was below the detection level of this technique. NB = no baseline could be estimated because of anomalously high Cl^- concentration. Resistivity-at-the-bit (RAB)-derived averages were calculated from pore water saturation estimates based on electrical resistivity data and tabulated at ~15-cm intervals and include hundreds of data points. These data require no correction for core recovery. No RAB data were acquired at Site 1252. RAB data are from the "A" hole at all sites, except from Site 1244, where they are from the "B" hole. Holes characterized by RAB data are ~50 m away from other holes at that site. All measurements in the GHOZ or GHSZ were included in the average, including data points indicating no gas hydrate. † = 88 mbsf is the depth at the bottom of this hole, which is ~24 m above the BSR.

Table T3. Summary of thermal gradients and heat flow.

Site	Water depth (m)	*N* T_o estimates (*N* attempts)	R^2 of line fit to the data	Thermal gradient (°C/km)	Seafloor intercept (°C)	Apparent standard error of data	Average thermal conductivity (W/[m·K])	Heat flow (mW/m²)
204-								
1244	895	13 (13)	1	62 ± 1	3.9 ± 0.1	0.12	0.93 ± 0.07	58 ± 5
1245	871	9 (12)	1	54 ± 1	4.1 ± 0.2	0.22	0.98 ± 0.05	54 ± 4
1246	851	5 (5)	0.95	55 ± 7	4.8 ± 0.5	0.46	0.93 ± 0.07	51 ± 10
1247	830	5 (7)	1	53 ± 1	4.2 ± 0.1	0.08	0.96 ± 0.07	51 ± 5
1248	830	4 (6)	1	54 ± 1	4.2 ± 0.1	0.04	0.98 ± 0.07	53 ± 5
1249	780	8 (2)	0.98	59 ± 3	4.3 ± 0.3	0.18	0.93 ± 0.07	55 ± 7
1250	790	12 (13)	0.98	59 ± 2	4.0 ± 0.2	0.27	0.94 ± 0.07	55 ± 6
1251	1212	7 (9)	1	54 ± 1	4.0 ± 0.1	0.2	0.83/0.95	49 ± 5
1252	1040	5 (6)	1	57 ± 1	3.5 ± 0.1	0.07	0.84/0.93	49 ± 4

Notes: Table from **Tréhu,** this volume. *N* = number of measurements.

CHAPTER NOTE*

N1. Abegg, F., Bohrmann, G., Freitag, J., and Kuhs, W., submitted. Fabric of gas hydrate in sediments from the Hydrate Ridge—results from ODP 204 samples. *Geo-Mar. Lett.*

*Dates reflect file corrections or revisions.